12-2016

Continuous Long-Term Health Monitoring using Ultrasonic Wave Propagation

Ece Erdogmus
University of Nebraska-Lincoln, eerdogmus@unl.edu

Project Title

Continuous Long-Term Health Monitoring using Ultrasonic Wave Propagation

Submitting Principal Investigators

Principal Investigator: Ece Erdogmus, PhD

December 2016

Table of Contents

ABBREVIATIONS

AASHTO	American Association of State Highway and Transportation Officials
GPR	Ground Penetrating Radar
DOT	Department of Transportation
IE	Impact Echo
NDOR	Nebraska Department of Roads
NDT	Non-Destructive Testing
UGW	Ultrasonic Guided Wave
UGWL	Ultrasonic Guided Wave Leakage
UPA	Ultrasonic Pulse Attenuation
UPV	Ultrasonic Pulse Velocity
UWP	Ultrasonic Wave Propagation

List of Figures

List of Tables

1. Introduction

This report presents the findings of a research project on using ultrasonic testing to continuously monitor reinforced concrete bridge decks for the onset of delamination. The report first presents a review of current nondestructive testing techniques used in practice and research, and deficiencies of these methods. Then the novel method developed in this project to identify early delamination in reinforced concrete bridge decks is presented. This method uses a unique sensor setup compared to current ultrasonic testing methods and utilizes the waves leaked into the concrete from the rebar that is excited with ultrasonic waves.

1.1. Problem Statement & Research significance

Due to the harsh loading and environmental conditions that reinforced concrete bridge decks are exposed to on a continuous basis, they are highly susceptible to constant and severe deterioration that can significantly threaten the quality, serviceability, and longevity of the system. The most common flaw found in reinforced concrete decks is delamination, particularly around the steel reinforcement. Delamination in reinforced concrete is a flaw which describes the splitting of concrete, or separation between the concrete and the embedded steel. Delamination around rebar can occur due to the corrosion of steel, which can cause stresses on the concrete surrounding the reinforcement, leading to crack formation. Reinforced concrete bridge decks are highly susceptible to this type of deterioration because of the common presence of chloride salts, moisture, and oxygen in the environment. In the United States, state departments of transportation (DOT) commonly utilize various non-destructive testing techniques (NDT) such as ground penetrating radar (GPR), impact echo (IE), and ultrasonic

testing (UT) to detect delamination in bridge decks. Currently, all DOTs only utilize the NDT techniques to detect already existing delamination and do not have techniques or methods to monitor the onset of delamination, therefore struggle to locate them before they become a serious issue. Each of the currently used NDT techniques to detect delamination in reinforced concrete bridge decks has their own advantages and disadvantages.

The driving ***hypothesis*** of this research is that an NDT method that involves ultrasonic wave propagation (UWP) and a specific sensor arrangement has the potential to identify the onset of delamination successfully. Ultrasonic testing methods provide very small wavelengths that can be utilized to detect micro-cracks, which is necessary to effectively identify the onset of delamination before it becomes a serious structural issue. However, the ultrasonic testing method commonly utilized is ultrasonic pulse velocity (UPV) and it has several drawbacks. It is labor intensive and a slow process due to the limitation of being able to examine only small areas at once and it is only sensitive to larger changes in conditions.

If the findings of the proposed research prove the hypothesis to be true, the method can be developed to be used for early detection of delamination in bridge decks before more serious problems develop. This research project presents the proof of concept studies and identifies the future work. The significance of this concept include: a new NDT method that can identify the onset of delamination before it becomes a serious structural issue, simplify the post-processing of data, and examine larger areas at once, which all can significantly contribute to healthier infrastructure and lowering maintenance cost.

1.2. Objectives

The ultimate goal of the project is to develop a novel method using ultrasonic wave propagation (UWP) *to identify the onset of rebar delaminations and to provide continuous health monitoring for the structure.*

This project involved an experimental program with two specimen sets. Each experimental set was designed for a specific set of objectives to help accomplish the ultimate goal:

Specimen Set 1 Objectives :

- To examine different test set-ups and sensor arrangements (existing and novel) in their effectiveness to identify onset of delamination
- To compare amplitude measurements and velocity measurements in their ability to identify onset of delamination.

Specimen Set 2 Objectives:

- To examine the ability of the proposed method monitoring leaked waves to identify delamination length and width.
- To determine the capabilities and distance limitations of the proposed method.
- To examine the correlation between amplitude and velocity measurements with respect to delamination width and length.

1.3. Research Plan & Tasks

The following project tasks were performed to achieve the research objectives:

1. Project Kick-of Meeting with the TAC: The meeting was held at the NDOR offices in July of 2015 and future directions for the project and all project tasks were discussed in detail.

2. Literature Search: A review of literature was carried out, in order todetermine the most appropriate test parameters, to successfully design the experiments, and to provide benchmarks and comparisons. Typical concrete deck details and concrete mixture characteristics were acquired from NDOR during this stage to aid in the design of experiments. A summary of the results of this task are presented in Chapter 2.

3. ***Design of Experiments & Meeting with TAC:*** Test parameters, test materials, as well as the number and size of the specimens for the first round of testing were determined by the project team based on the results of the literature search and consultations with the TAC.

4. Experimental Program- Specimen Set 1: All experimental work was conducted in the Peter Kiewit Institute (PKI) structures laboratory (PI's home laboratory in Omaha), using a reinforced concrete slab-like specimen.

5. 50% Completion Meeting with TAC: The data and findings from the first set of experiments were presented and discussed at the 50% completion meeting. Details of the second experiment set were also discussed.

6. Experimental Program- Specimen Set 2: A second set of testing was carried out. This set of experiments focused on refinements to the project method, such as optimization of the number and location of instrumentation.

7. Conference and/or journal paper preparation and presentation: The data collected, studied, and discussed with TAC was summarized in two journal articles, both of which are currently under review.

8. 75% Completion Meeting with TAC: TAC was updated on the results at this meeting.

9. Completion of final report: The findings of the project are presented in this document, which is the final report.

10. Completion of technical brief: A one page summary of the project and its findings will be prepared in a news release type format to be used for research dissemination and promotion by NDOR and UNL.

11. Final presentation to NDOR: A final presentation was given to the NDOR representatives in the fall of 2016.

2. Review of Literature: Nondestructive testing on reinforced concrete for delamination

2.1 Bridge Assessment and Repair Trends

The National Cooperative Highway Research Program (NCHRP) conducted a nationwide study in 2009 investigating the rehabilitation and maintenance methods used by State Department of Transportations (DOTs) (Krauss et al., 2009). The study found that the most common response to reinforced concrete bridge deck delaminations were overlays or deck replacement, which are expensive and time consuming. Floodcoats, a slightly cheaper and less time consuming rehabilitation method has slowly gained popularity; however, they are only effective as sealers for cracks or delaminations, making them applicable only if damage is detected early (Krauss et al., 2009; Rogers et al., 2011). A detailed discussion about application and types of floodcoats is presented in (Rogers et al., 2011).

The same nationwide research also investigated the evaluation techniques used by DOTs to examine bridge deck conditions (Krauss et al., 2009). Based on the results of 46 DOTs' responses, qualitative methods such as visual inspections, hammer sounding, and chain dragging are the most commonly practiced evaluation techniques by DOTs to assess bridge deck conditions. Although these relatively simple methods require trained and experienced inspectors, a large amount of time to perform, and can only provide a *qualitative* assessment of the condition of the concrete, they remain popular because they are inexpensive and simple. With relatively recent advancements in imaging technologies, acoustics, and electromagnetics, NDT methods such as ground penetrating radar (GPR), ultrasonic pulse velocity (UPV), and impact echo (IE) have also gained recognition. According to Krauss et al. (2009), these NDT

techniques are not often utilized by DOTs despite their ability to provide quantitative information because they are inefficient in terms of cost and time compared to qualitative methods. A comprehensive study detailing and comparing all currently practiced quantitative NDT methods used on bridges decks can be found in the National Research Council (NRC) and Second Strategic Highway Research Program (SSHRP) document from 2013. Amongst quantitative NDT methods, GPR, IE, and UPV have been found to be the most effective methods in assessing the condition of bridge decks, particularly when used together (Clemena et al., 2000; Cui et al., 2012; National Research Council (U.S.) and Second Strategic Highway Research Program (U.S.), 2013; Zhu, 2008). Despite the lack of common use by DOTs, technological developments of quantitative NDT methods have been encouraged in recent years. Such a technological development includes the RABIT™ bridge deck assessment tool developed by FHWA and CAIT which collects comprehensive data of the surface and subsurface conditions automatically and simultaneously (FHWA, 2014b). The RABIT™ bridge deck assessment tool uses a combination of GPR, IE, ultrasonic surface waves, GPS, and high definition imaging. The RABIT™ bridge deck assessment tool is a tremendous development in NDT for bridge decks and has been used in the assessments of bridges nationwide. Another NDT technology that has been developed is the MIRA ultrasonic low-frequency tomographer which provides high resolution images for reinforced concrete (ACS, 2014; Cui et al., 2012). Even though these technological advancements providing high-resolution images and spot-checks with NDTs are exciting, there remains a gap for a method that can provide continuous and global health monitoring for bridge decks to identify *the onset of delamination*. In order to effectively improve maintenance protocols, the condition of the bridge decks need to be continuously

monitored, thus allowing for preventative measures (National Research Council (U.S.) and Second Strategic Highway Research Program (U.S.), 2013). Current NDTmethods used on bridge decks do not have the ability to identify the onset or early stages of delamination effectively. Despite the possibility of cheaper repair methods in the case of early detection, damage is typically only found when the reinforced concrete bridge decks require a more costly intervention.

2.2 Ultrasonic Testing

UPV is an NDT method standardized by the American Society for Testing and Materials (ASTM) and is commonly used for concrete inspection (ASTM, 2009). The technique is based on the velocity measurements of the longitudinal stress waves propagating through the structure. Using UPV, based on the density, dynamic modulus of elasticity, and Poisson's ratio of the structural materials, theoretical velocities can be determined and compared to the measured velocities (ASTM, 2009; Naik et al., 2004). A difference between these velocities indicates either changes in material (E, ρ, ν) or an anomaly (i.e. a delamination) interrupting the direct path between the source and receiver. Various studies, such as those done by Kumar et al. (2006) and Hassan et al. (1993), have demonstrated that different arrangements differ in sensitivity to flaws or anomalies. The capabilities and limitations of the UPV testing method to characterize the properties and conditions of concrete have also been studied extensively. The path length between transducers has been found to influence accuracy of results in practice, despite it being theoretically independent of propagation time. According to the *Reunion Internationale des Laboratoires et Experts des Materiaux, Systemes de Construction et Ouvrages* (RILEM). the recommended path length between transducers in a UPV test arrangement is 0.5ft to 5ft

(RILEM TC, 1994). They also recommend minimum path lengths to be used when testing concrete related to specified maximum aggregate sizes. These path lengths are suggested because smaller path lengths have a tendency to give greater pulse velocities because of the inhomogeneous nature of concrete (Naik et al., 2004; RILEM TC, 1994). However, Kumar et al. (2006) found inaccuracies in determining crack location when the path length was greater than 4in. for the indirect test arrangement (most commonly used arrangement for bridge deck assessments, which is presented in Section 3.3), suggesting that the aforementioned RILEM recommendations should be further researched.

For reinforced concrete, another influencing factor to UPV results is that elastic stress waves travel 1.4 to 1.7 times faster in steel compared to concrete; therefore, velocity measurements can be difficult to interpret when steel reinforcement is embedded in concrete. UPV standards set by ASTM, RILEM, and the British Standards Institute (BSI) recommend avoiding areas with steel reinforcement in UPV testing (ASTM C597-09, 2009; Naik et al., 2004; RILEM TC, 1994). If unavoidable, RILEM and the BSI do provide velocity based correction factors if steel reinforcement is present (Naik et al., 2004; RILEM TC, 1994). However Lencis et al. (2011) found that the presence of steel reinforcement in concrete can cause reductions in ultrasonic pulse velocities, contradicting other studies and various standards. This demonstrates that the standardized methods should be further researched. Naik et al. (2004) provides a comprehensive summary discussing the background, theory, method, influential factors, and studies of application of UPV. For concrete, the UPV method has been demonstrated to be a tool that can be used to estimate strength of concrete (Hassan et al., 1993; Naik et al., 2004;

Sabnis et al., 1990), homogeneity of concrete (Hannachi and Guetteche, 2014; Naik et al., 2004), hydration of cement (Naik et al., 2004), durability of concrete (Naik et al., 2004), density of concrete (Naik et al., 2004), surface crack depth (Kumar and Santhanam, 2006; Naik et al., 2004; Sabnis et al., 1990), and dynamic modulus of elasticity (Naik et al., 2004; Sabnis et al., 1990).

Although this method is primarily based on velocity measurements, attenuation measurements have been found by several research studies to be more sensitive to interior defects in mixed media (Butt et al., 2004; Goueygou et al., 2002; Huang et al., 2014; Kee and Zhu, 2013; Landis and Shah, 1995; Santhanam, 2010; Shah and Hirose, 2009; Streeter, 2002; Suaris and Fernando, 1987; Treiber et al., 2010). Despite being more sensitive to deterioration, the method using attenuation measurements, which some have referred to as Ultrasonic Pulse Attenuation (UPA) (Kee and Zhu, 2013; Santhanam, 2010; Suaris and Fernando, 1987), is not a standardized testing method. Streeter (2002) found that attenuation measurements could be orders of magnitude more sensitive to anomalies such as steel or low density concrete than velocity measurements. Kee and Zhu (2013) also demonstrated this, finding that UPA measurements decreased by 90%, while UPVs only dropped by 20-30% with respect to the development of a crack. Butt et al., (2004) performed a study that utilized the semi-direct approach and found that monitoring the changes in attenuation can be a reliable and sensitive indicator of fatigue cracking in a steel-free deck. However, they found that the location of the damage was difficult to identify and damage was quantified with respect to load cycles. Suaris and Fernando (1987) also performed cyclical loading tests on concrete and found that the relationship between attenuation and

damage accumulation is not linear, particularly during the initial cycles. Shah and Hirose (2009) used amplitude measurements of a nonlinear UT method and second harmonic generation to detect damage prior to standard UPV methods. Shah and Hirose (2009) used the ultimate compressive strength of concrete as the indicator of damage level and found that velocity measurements were only sensitive to damage levels exceeding 60% of ultimate strength. Dumoulin et al. (2014) and Song et al. (2007) developed damage indexes using the root mean square deviation between the amplitude of a healthy and damaged signal computed in the corresponding time window. The equation they used for the damage index implies that there is no damage unless there is a change in velocity, suggesting that velocity is the more sensitive measurement. They also examined the relationship between the damage index (a function of attenuation and velocity) to load. The UPA method has also demonstrated the potential ability to quantify or indicate characteristics of cement based materials, such as entrained air void size, water-cement ratio, and homogeneity (Dumoulin et al., 2014; Hannachi and Guetteche, 2014; Huang et al., 2014).

UT with concrete can experience two types of attenuation: intrinsic and extrinsic. Intrinsic attenuation is caused by the medium through which the elastic waves are travelling, as a result of scattering and absorption caused by aggregates or voids. Extrinsic attenuation describes attenuation caused by anything other than the body being examined, such as coupling. Coupling is a major reason why attenuation measurements are not yet a standard practice because it is a variable that is very difficult to control and has a significant influence on energy transmission between the transducers. This has led to the recent development of embeddable

transducers in concrete to allow coupling conditions to be fixed, thus theoretically eliminating the influence it has on continuously monitored data. Several studies have developed or used embedded transducers to monitor damage to concrete (Annamdas et al., 2010; Chen et al., 2006; Dumoulin et al., 2014; Huang et al., 2014; Kee and Zhu, 2013; Niederleithinger et al., 2015; Song et al., 2007).

2.3 Ultrasonic guided waves

Ultrasonic guided waves (UGW) propagate when boundaries are present and are close together, thus cause the ultrasonic waves reflected at the boundaries to result into a superimposed wave form that travels along the wave guide. The guided wave is just a sum of all of these reflected waves, including amplitude and phase information.

Thus far the UGW based testshave been used in practice mostly on steel pipes and have been showed to travel distances of 50 feet or more. However, this is only the case when the pipes are not embedded (the waveguide is the pipe and the surrounding medium is air), which allows the majority of the waves to reflect back into the waveguide at the steel-air interface due to large differences in impedance between these materials. In a reinforced concrete structure, the embedded steel reinforcing bar can be utilized as a cylindrical waveguide, but due to the impedance difference between steel and concrete being less than that of steel and air, more wave energy is refracted at the steel-concrete interface which causes the guided wave to attenuate much faster. Leakage of energy into surrounding material is typically viewed as a disadvantage of UGW as it diminishes the prime advantage of the technique: which is propagation distance. For reinforced concrete structures, the UGW method has recently gained

the interest of researchers due to its ability to inspect greater distances than conventional NDE methods used for concrete examination, but this method requires access to the steel bars. A guided wave travelling through a cylindrical steel bar embedded in concrete is an example of what is called a leaky cylindrical guided wave, where bulk waves leak out of the waveguide and radiate into the surrounding material (Pavlakovic, 1998). The energy leaked out consequently causes the guided wave to attenuate.

Both bulk longitudinal (P-wave) and shear (S-wave) waves can leak out of a waveguide and radiate into the surrounding material if the embedding material is a solid (Pavlakovic, 1998; Vogt, 2002). The type of leaked wave is dependent on the how the phase velocity of the guided wave compares to the velocity of the longitudinal and shear waves that travel in the embedding material (Pavlakovic, 1998). Depending on the material properties, geometry, frequency and mode, a guided wave system embedded in a solid material can be one of the following:

a) Non-leaky – this only occurs when the phase velocity of the guided wave is less than the shear velocity of the embedding material.

b) Leak only bulk shear waves – this occurs when phase velocity of the guided wave is greater than the shear velocity of the bulk wave and less than the longitudinal velocity of the bulk wave.

c) Leak both longitudinal and shear bulk waves – which occurs when the phase velocity of the guided wave is greater than both the longitudinal and shear velocity of waves in the embedding material.

In a reinforced concrete system where the steel bar is used as the waveguide, ultrasonic waves will reflect and refract at the steel and concrete interface. The reflected waves cause guided waves to form, while the refracted waves are the waves that leaked out into the surrounding concrete. Snell's law describes the relationship between the angles of incidence and refraction of waves passing through a boundary between two materials (Equation 1).

$$\frac{\sin\theta_1}{\sin\theta_2} = \frac{c_1}{c_2} = \frac{\lambda_1}{\lambda_2} \quad (1)$$

The angle that these bulk waves leak out into surrounding material can be calculated using Snell's law, where the incident angle (θ_1) is 90° (the direction of the propagating guided wave), c_{concrete} and c_{phase} correspond to c_1 and c_2, respectively, and θ_{leakage} is the angle of refraction (θ_2). Leakage angle can be calculated using Equation 2 and is illustrated in Figure 1.

$$\theta_{\text{leakage}} = \sin^{-1}\left(\frac{c_{\text{concrete}}}{c_{\text{phase}}}\right) \quad (2)$$

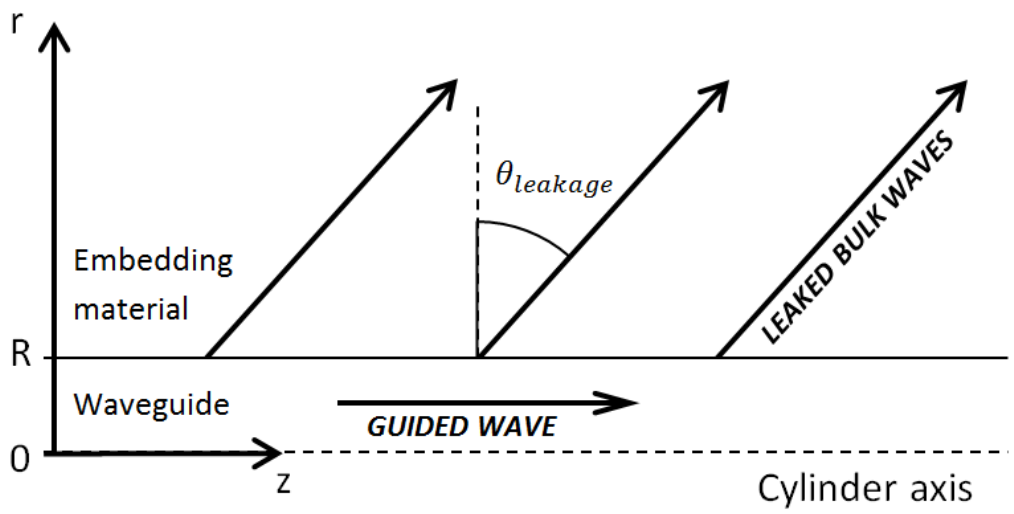

Figure 1– Leakage of bulk waves

In almost all of the studies that utilize UGW, an ultrasonic transmitter and a receiver are placed at the ends of the reinforcing bar, thus examine the guided wave and not the leaked waves. Some test arrangements used only one transducer and detected the reflected signal from the other end of the bar (pulse-echo technique). A few studies attached transducers to actuate and receive the signal at certain points along the reinforcing bar (Wang et al., 2009; Zhu and Hao, 2009), developing a completely embedded system. Most UGW studies on reinforced concrete have used lower ultrasonic frequencies (less than 150kHz) (Ervin, 2007; Li et al., 2014, 2012; Lu et al., 2013; Mustapha et al., 2014; Na et al., 2003; Vogt, 2002; Wang et al., 2009; Wu and Chang, 2006; Zheng and Lei, 2014; Zhu and Hao, 2009). This is because lower frequencies are more sensitive to bond conditions and are less complex problems to solve. Lower ultrasonic frequencies often only propagate the fundamental modes: L(0,1), T(0,1) and F(1,1), following the notation set by Silk and Bainton (1979) discussed in subsection 3.1. At higher frequencies, the presence of numerous waveguide modes complicates analysis significantly and different

modes may interfere (Vogt, 2002). It is generally understood that the energy of some wave modes progressively becomes more concentrated at the center of the reinforcing bar as excitation frequency increases. Hence these modes are less sensitive to the bond conditions between steel reinforcement and concrete, but also less susceptible to energy leakage (Ervin, 2007; Lu et al., 2013; Pavlakovic, 1998). Since higher ultrasonic frequencies have been found to be generally less susceptible to leakage, they have also been studied with the primary goal to increase the inspection range of UGW for embedded steel reinforcing bars (Ervin, 2007; Miller, 2010; Na et al., 2003; Pavlakovic, 1998; Zheng et al., 2014).

Numerous studies have demonstrated the ability of UGW in detecting or monitoring the bond condition between steel reinforcement and concrete. The majority of studies have examined the ability of UGW to detect debond at the steel-concrete interface by casting specimens with built-in delamination of known lengths (Li et al., 2012; Miller, 2010; Mustapha et al., 2014; Na et al., 2003; Wang et al., 2009; Wu and Chang, 2006; Zhu and Hao, 2009). All of these studies found that as debond length increased, the amplitude of the transmitted signal increased. Zhu and Hao (2009) also found that velocity increased as debond length increased and that the velocity of guided wave was not influenced by excitation frequency in the range of 30 to 80kHz. Wu and Chang (2006) demonstrated that the amplitude of the received signal increases exponentially with debond length and developed an equation to estimate its length. However, the delamination width did not affect the sensor output and thus cannot be estimated with the equation. Wu and Chang (2006) also found that small sized cracks inside the concrete structure do not affect sensor output. Wang et al. (2009) developed a numerical model and conducted an

experimental study which illustrated that debond location can be estimated using velocity measurements. Na et al. (2003) demonstrated that frequencies varying from 50 kHz up to 1MHz are effective at indicating the presence, and are sensitive to the size, of a delamination using amplitude measurements, but delamination location cannot be identified using amplitude readings. Li et al. (2012) determined that higher strength concrete caused more leakage of energy. Mustapha et al. (2014) developed a time-reversal process method that proved effective in identifying damage at the steel-concrete interface. In addition to detecting debond, Miller (2010) examined the ability to monitor corrosion and found that increases in corrosion reduced the guided wave amplitude. Miller (2010) also developed an effective time of flight method to monitor corrosion of an embedded steel reinforcing bar, which is not affected by amplitude, hence is also not affected by the transducers coupling. Miller (2010) also found that reinforcement type (type of ribs) influences the rate of leakage and that waveguides with greater diameters attenuate slower. Ervin (2007) also monitored corrosion using both low and high ultrasonic frequencies. This study examined steel reinforcement embedded in mortar. The low ultrasonic frequency signal (L(0,1) mode) highly attenuated due to leakage, but it was sensitive to combined effects of bond deterioration and mortar stiffness reduction. The high ultrasonic frequency (L(0,9) mode) was insensitive to the surrounding interface, which allowed for pitting corrosion to be monitored and the results were isolated to just the steel bar cross section. Ervin (2007) found that the guided wave signal is attenuated as the corrosion initially accumulates between the steel and the mortar. The corrosion product created a higher bond level (i.e. increase in coupling), causing wave energy to leak out of the bar into the surrounding mortar at a higher rate. The UGW signal began to gain strength after the pressure reached an

apex and caused the mortar to crack. Based on dispersion curves, Li et al. (2014) determined that the fundamental longitudinal mode (L(0,1)) at 40kHz should be recommended for testing reinforced concrete corrosion damage. Li et al. (2014) found that when monitoring pitting corrosion, there is first a slight increase in amplitude (debond) before gradual decrease (pitting corrosion causing damage to steel). Zheng and Lei (2014) examined the effects that concrete has on the propagation of the guided wave travelling through an embedded reinforcing bar. Zheng and Lei (2014) found that attenuation dispersion curves are influenced by the concrete's properties, while velocity does not show the same effect. The shear modulus ratio and density ratio between the steel and concrete only influence the attenuation of guided wave due to leakage. Zheng and Lei (2014) found that lower shear modulus, strength, density, and larger reinforcing bar diameter increase transmission distance. Vogt (2002) examined the ability of UGW to determine the material properties of the concrete. Vogt (2002) focused on the L(0,1) mode and used two methods: attenuation and reflection. Using both methods, Vogt (2002) found that shear properties of the embedding material can be determined. Rose (2003, 2002) summarizes the basic knowledge of dispersion curves as it pertains to guided wave analysis and provides a summary of the fundamental theory and practice of UGW inspection.

2.4. Summary of Literature Review: Research Gaps

Table 1 summarizes what has been done in terms of research and what has been utilized in practice by DOTs regarding bridge deck inspection for delamination.

Table 1 – Summary of what has been done in terms of research and what is done in practice by DOTs regarding *bridge deck inspection* for delamination:

Bridge Deck Inspection	**UPV**	**UGW**	**Other NDT**
Detect Delamination	Practice: Yes Research: Yes	Practice: **No** Research: **No** *(Yes in RC, not specifically bridge decks)*	Practice: Yes Research: Yes
Monitor **onset** of cracking	Practice: **No** Research: Yes (unreinforced concrete deck)	Practice: **No** Research: **No**	Practice: **No** Research: Yes
Monitor **onset** of debond	Practice: **No** Research: **No**	Practice: **No** Research: **No** *(Yes in RC, not specifically bridge decks)*	Practice: **No** Research: **No**
Monitor **onset** of corrosion	Practice: **No** Research: **No**	Practice: **No** Research: **No** *(Yes in RC, not specifically bridge decks)*	Practice: Yes Research: Yes
Embedment	Practice: **No** Research: **No** *(Yes in RC, not specifically bridge decks)*	Practice: **No** Research: **No** *(Yes in RC, not specifically bridge decks)*	-
Path Range	Recommended Practice: 0.5'-5'	Studies of embedded steel: 6'-15'	Varies
Attenuation vs. Velocity	Practice: Velocity Studies: Attenuation	Attenuation	-
Expertise required	Yes	Yes	Typically Yes
Examine Concrete and steel at once	**No**	Yes ***(not really utilized)***	-

3. Experimental Approach

3.1. Choice of guided and leaked wave modes

In any guided wave study it is important to understand how excitation frequency influences the propagation of the different modes in the waveguide. Since this study examines the influence

that deterioration has on both amplitude and velocity measurements, and due to the fact that longitudinal modes generally propagate the fastest and affect the arrival time of signal, only longitudinal guided wave modes were considered for the experimental study. However, as mentioned earlier, leaked waves can propagate as both longitudinal and shear waves.

Using the material properties shown in Table 2 and the program developed by Sun and Zhu (2017), the longitudinal attenuation and velocity dispersion curves (shown in Figures 2 and 3, respectively) for the embedded guided wave system used in the experimental study were modelled. The longitudinal velocities stated in Table 2 were experimentally calculated. They were the average velocities of 54 kHz ultrasound pulses propagating through six #5 steel bars that were two feet long each and nine 4in. x 8in. concrete cylinders.

Table 2- Model Parameters

Material (Layer)	**Radius of cylindrical layer (m)**	**P-wave Velocity (m/s)**	**Poisson's ratio**	**Density (kg/m^3)**
Steel (Inner)	$7.9375*1e^{-3}$	5850	0.3	7932
Concrete (Outer)	Infinite	3978	0.2	2200

Only the fundamental longitudinal mode propagates when the frequency is less than 270 kHz, and within the range of 40 and 125 kHz the fundamental longitudinal mode has low attenuation due to leakage, as shown in Figure 2.

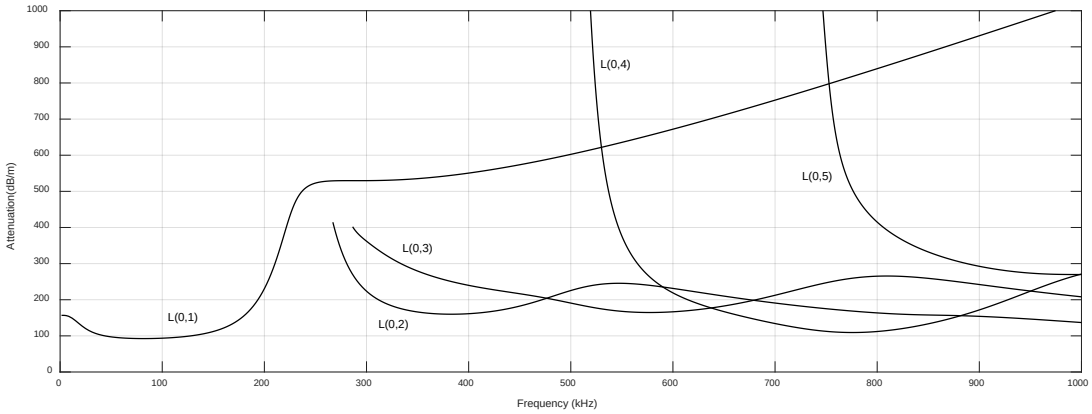

Figure 2 – Attenuation dispersion curves of longitudinal modes of guided wave in steel bar embedded in concrete

Figure 3 shows the phase velocity dispersion curves of the guided wave longitudinal modes modelled using the parameters shown in Table 2. The two horizontal dashed lines, which divide the plot into regions, are the longitudinal and shear velocities of ultrasound in the embedding material, in this case concrete. These regions can be used to identify if modes are non-leaky, leak out shear bulk wave, or leak out longitudinal and shear bulk waves (Pavlakovic, 1998). Figure 3 suggests that the L(0,1) mode would leak both longitudinal and shear bulk waves if frequencies were less than 270 kHz, and that only shear bulk waves would be leaked if frequencies were greater than 270 kHz. However, even though the L(0,1) mode only leaks out shear waves at frequencies above 270 kHz, other longitudinal modes are also excited at those frequencies as the guided wave disperses. This would cause the L(0,1) mode to leak out shear waves and the other longitudinal modes to leak longitudinal and shear bulk waves of their own simultaneously. So despite two types of leaked bulk waves simultaneously propagating through

the concrete when the L(0,1) is excited at using frequencies below 270 kHz, frequencies below 270 kHz provides the scenario with the least number of the guided and leaked wave modes.

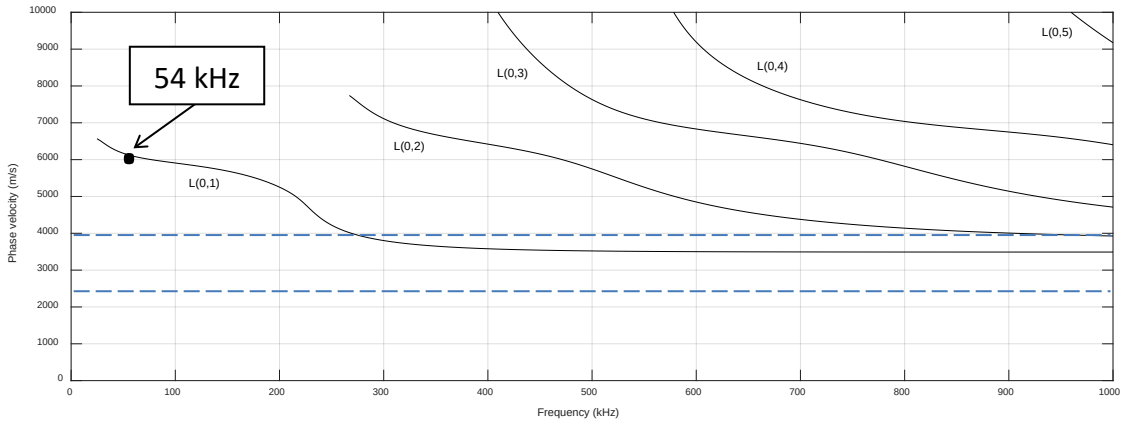

Figure 3 – Phase velocity dispersion curves of longitudinal modes of guided wave in steel bar embedded in concrete

The choice of the excitation frequency was determined by considering how it would influence the attenuation and dispersion of the guided wave, the type and number of leakage modes (influenced by dispersion of guided waves), and the intrinsic attenuation of bulk waves propagating in the surrounding concrete. The excitation frequency used in the experimental study was 54kHz, which excites only the fundamental longitudinal mode L(0,1) in the waveguide, and is in the range of frequencies that minimizes both attenuation of the guided wave and bulk waves. For the selected 54 kHz excitation frequency, both longitudinal and shear bulk waves will leak out into the concrete. 54 kHz transducers are commercially available and one of the most commonly used frequencies of ultrasonic testing equipment designed for standardized ultrasonic testing of concrete.

3.2. Experimental set-up

The general experimental set-up used to collect monitored data for all specimens is shown in Figure 4. The experimental set-up included two parts: 1) a transmitting part (T), a standard 54 kHZ transducer and 2) a piezoelectric sensing part (R), which was either a 2 inch diameter transducer or pinducer (miniature transducer) from CTS Valpey corporation. A low noise preamplifier was used to amplify the signals detected by pinducers. The handheld data acquisition system NDE 360 platform from Olson Instruments was used to generate and collect ultrasonic signals.

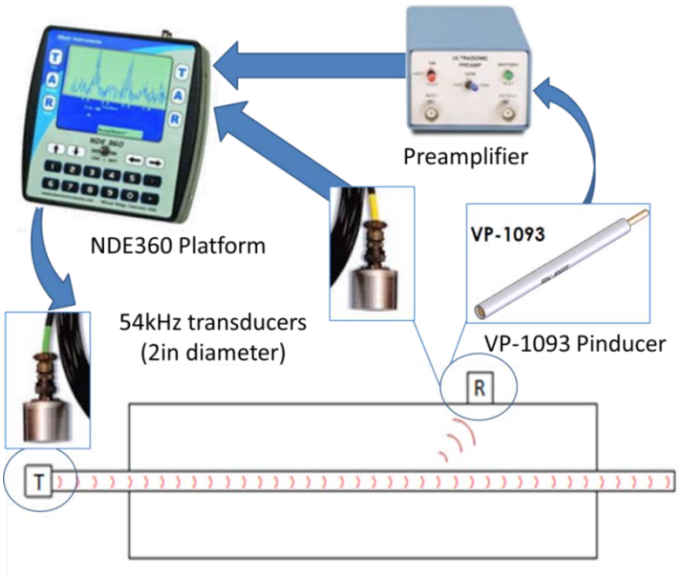

Figure 4. Experimental set-up

3.3. Ultrasonic testing arrangements

All test specimens examined the ability of four different test arrangements to identify the onset of delamination. Three of the test arrangements (Figure 5a, b and c) have been previously used to some degree. The fourth test arrangement (Figure 5d) investigated is novel to this study and

detects the ultrasonic guided wave leakage (UGWL). Transmitting a guided wave through a steel reinforcing bar allows for long propagation range and no attenuation due to scattering caused by aggregates; while detecting the leakage allows for simple analysis of bulk waves.

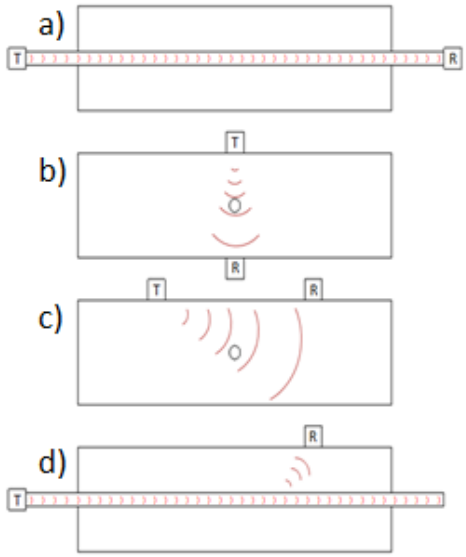

Figure 5. Test arrangements

3.4. Data Collection

During the monitoring process, data was collected with respect to incremental changes in crack /delamination size. Before introducing deterioration to the reinforced concrete specimens, baseline data was collected using the UGWL arrangement. The tests would then be repeated as deterioration was slowly introduced and the changes in collected readings would be analyzed.

The velocity and amplitude of signals were recorded and analyzed. The velocity of the signal was calculated using the arrival time of the signal, and the theoretical distance which was defined by the leakage angle of the longitudinal bulk waves. Theoretically, the guided wave

should leak out both longitudinal and shear bulk waves into the surrounding material. Figure 6 shows the leakage angles calculated using Equation 2.

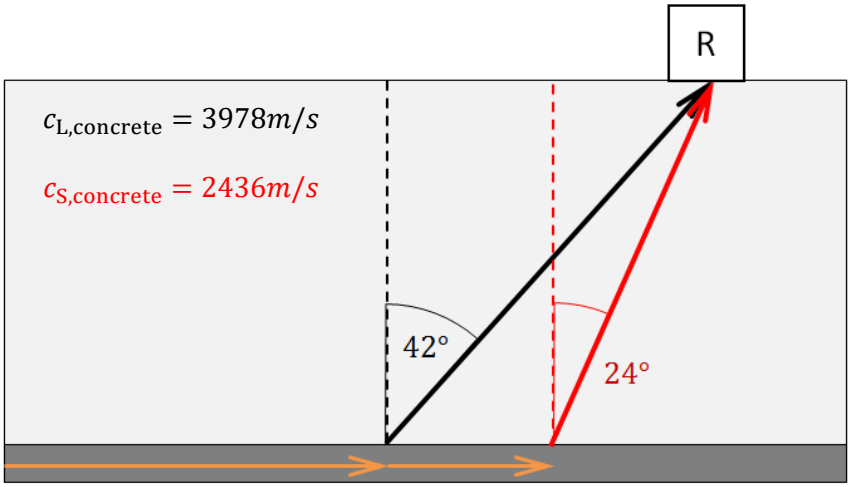

Figure 6 – Theoretical leakage angles

Using the velocities presented in Table 2 and Equation 2, the longitudinal and shear leakage angles were calculated to be 42° and 24°, respectively, as shown in Figure 6. Figure 6 illustrates how the paths of both types of leaked waves would reach a sensor. Theoretically, the longitudinal waves leaked out at a 42° angle would arrive at a sensor before leaked shear bulk waves do, therefore the 42° leakage angle was used to calculate the distance travelled. The arrival time of signals was determined from the data collected in the time domain, as shown in Figure 7, where the blue line would be the chosen arrival time of the ultrasound.

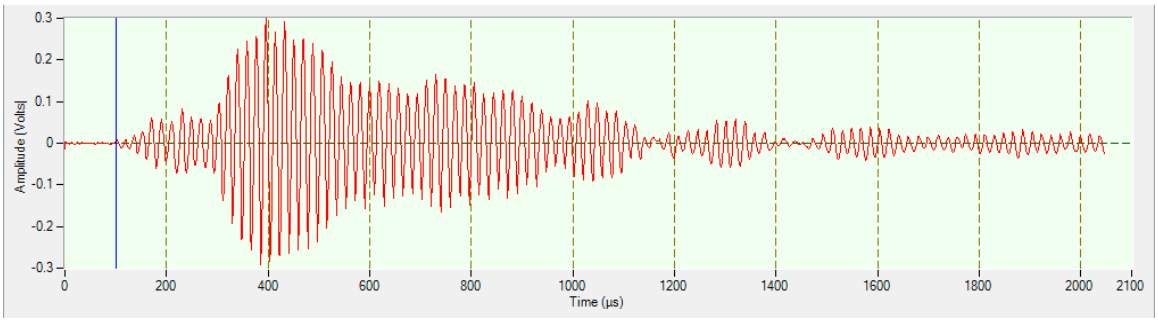

Figure 7 – 2 inch transducer in UGWL arrangement.

Amplitudes of the signal were not collected in the time domain since the guided wave system theoretically leaks out both longitudinal and shear bulk waves, which would reach a sensor at different times and impose on one another. The signal data was converted from the time domain to the frequency domain using a fast Fourier transform (FFT) to determine the amplitude. The amplitude was determined by reading the amplitude at the excitation frequency, 54 kHz, in the frequency domain. All waves propagating at a specified frequency, regardless of time, influence the amplitude of the specific frequency in the frequency domain plot. In the UGWL arrangement, both the longitudinal and shear bulk waves leaked out of the waveguide would contribute to the amplitude in the frequency domain, as both propagate at the excited frequency of 54 kHz. The FFT of the signal shown in Figure 7 is shown in Figure 8.

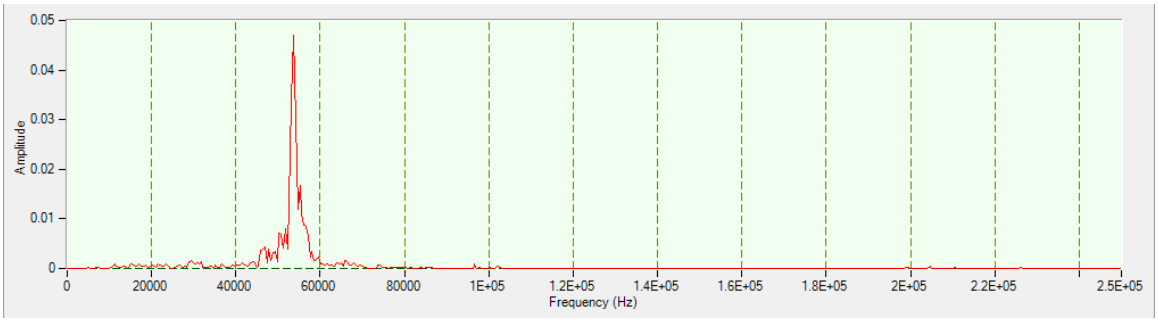

Figure 8 – Fast Fourier transform (FFT) of signal in Figure 7.

Data was collected every time test specimens were separated mechanically in gradual increments. For all specimens in the experimental study, each reading collected at each incremental stage of damage was repeated ten times.

For the post-processing of the collected data, the change of amplitude and change of velocity calculations were performed (Equations 3 and 4) and examined against delamination size.

$$Change\ of\ amplitude\ (\%) = \left(\frac{A_i}{A_0} - 1\right) \times 100 \tag{3}$$

Where:

A_i – is the amplitude of 54 kHz in the frequency domain at the i^{th} increment of delamination

A_0 – is the amplitude of 54 kHz in the frequency domain before delamination

$$Change\ of\ velocity\ (\%) = \left(\frac{V_i}{V_0} - 1\right) \times 100 \tag{4}$$

Where:

V_i – is the velocity of the signal at the i^{th} increment of delamination

V_0 – is the velocity before delamination

Distance used to calculate velocity is that of the path determined by the leakage angle.

In addition to the percent changes in measurements, the attenuation coefficients of the guided wave and the leaked waves in both the z-direction and leakage angle direction) were examined

in specimen set 2. The attenuation coefficient (α) describes the weakening of signal due to scattering or absorption, and can also be considered as the decay of power or intensity of a sound wave (Rose, 1999). It is defined by Equation 5:

$$A_i = A_0 e^{-\alpha(z-z_0)} \tag{5}$$

where A_i and A_0 are the decreased and initial amplitudes, respectively, and $z\text{-}z_0$ is the distance the wave has travelled through the material. When determining the attenuation coefficient of the guided wave, $z\text{-}z_0$ was the distance that the ultrasound travelled in the embedded steel bar (i.e. distance between transmitter and receiver located at ends of embedded bar). When determining the attenuation of the leaked waves, $z\text{-}z_0$ was the distance between the points along the array in the z-direction or the distance between arrays in the leakage angle direction. Attenuation coefficient can be determined by Equation 6 and typically uses the unit Np/m [Equation 7], which can be converted to dB/m using Equation 7.

$$\alpha = -\frac{\log_e\left(\frac{A_i}{A_0}\right)}{(z - z_0)} \tag{6}$$

$$1\frac{Np}{m} = 8.686\frac{dB}{m} \tag{7}$$

3.5. Test specimens

3.5.1. Specimen set 1

Specimen set 1 consisted of concrete specimens of 18”x18”x5” cast with a #5 steel rebar embedded at the center of the cross-section (Figure 9). The specimens were 5 inches so that

the cover of concrete over the steel reinforcing bar would be 2.5 inches, as found in in NDOR bridge decks. Specimens were cast in layers with a 2” strip of plastic at the start of the expected crack to promote crack propagation along rebar level. The crack was created and gradually increased mechanically with a device; as shown in Figure 10. The concrete mix design used for the test specimens is based on the Nebraska department of roads (NDOR), and is called 47BD. The concrete mix design is commonly used on their bridge decks and also meets the criteria set out by the *American Association of State Highway and Transportation Officials (*AASHTO) for concrete bridge decks. The specified compressive strength of the 47BD concrete mix design is 4ksi.

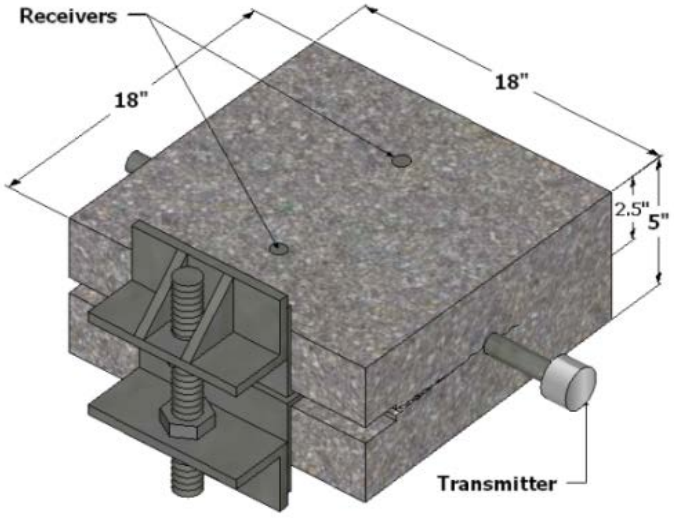

Figure 9. Specimen set 1 illustration

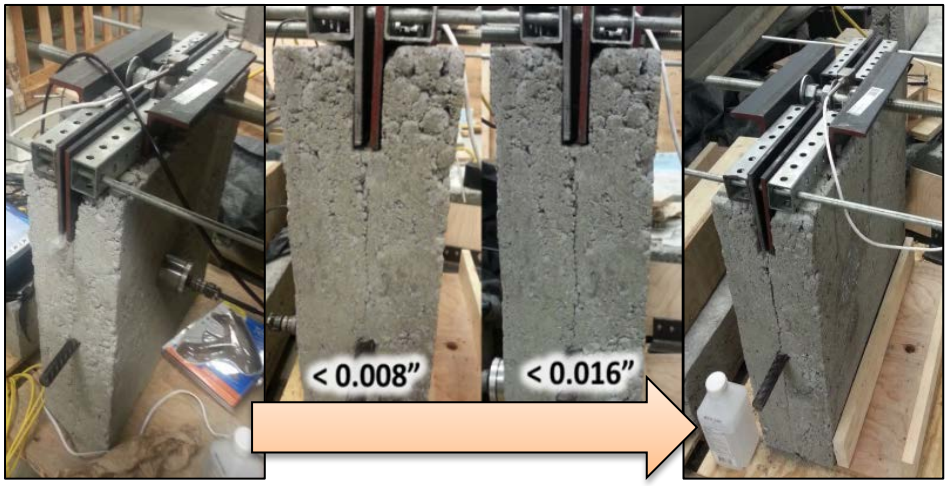

Figure 10. Gradual mechanical separation in increments of 0.008”

3.5.2. Specimen set 2

Specimen set 2 was composed of two identical concrete test specimens that were 66 inches x 18 inches x 5 inches cast with a No.5 steel reinforcing bar embedded as shown in Figure 11. Specimens were cast with plastic film strips on one end to promote crack propagation along the reinforcement level. At this end, a crack was created and gradually increased mechanically with the device shown in Figure 11, as done in specimen set 1 (Figure 10). The circles on specimen seen in Figure 11 were transducer locations, which are explained later in this section.

For all specimens, the transmitting transducer was fixed using hot melt glue as a couplant. The receiver was fixed using hot melt glue as a couplant during mechanically induced and natural crack growth. When crack growth appeared to have settled, grease was used as couplant for the receiver when collecting data from the arrays of sensor locations.

Figure 11. Specimen set 2

Specimen set 2 focused on examining the abilities of the proposed UGWL method. Figure 12 to 14 illustrate the transducer locations used in specimen set 2 and the paths of leaked ultrasound from the bar. Embedded guided waves propagating along a steel bar, i.e. the axial direction, attenuate as energy leaks out from the waveguide into the surrounding material. The leakage angle of the longitudinal bulk wave was calculated to be 42° using Snell's law, as shown in section 3. Arrays of transducer locations in the z-direction at various different distances from the embedded steel bar were examined. Each array had transducer locations to monitor specific points along the steel bar (i.e. 6 inches, 12 inches, 18 inches etc…) which were determined using the leakage angle.

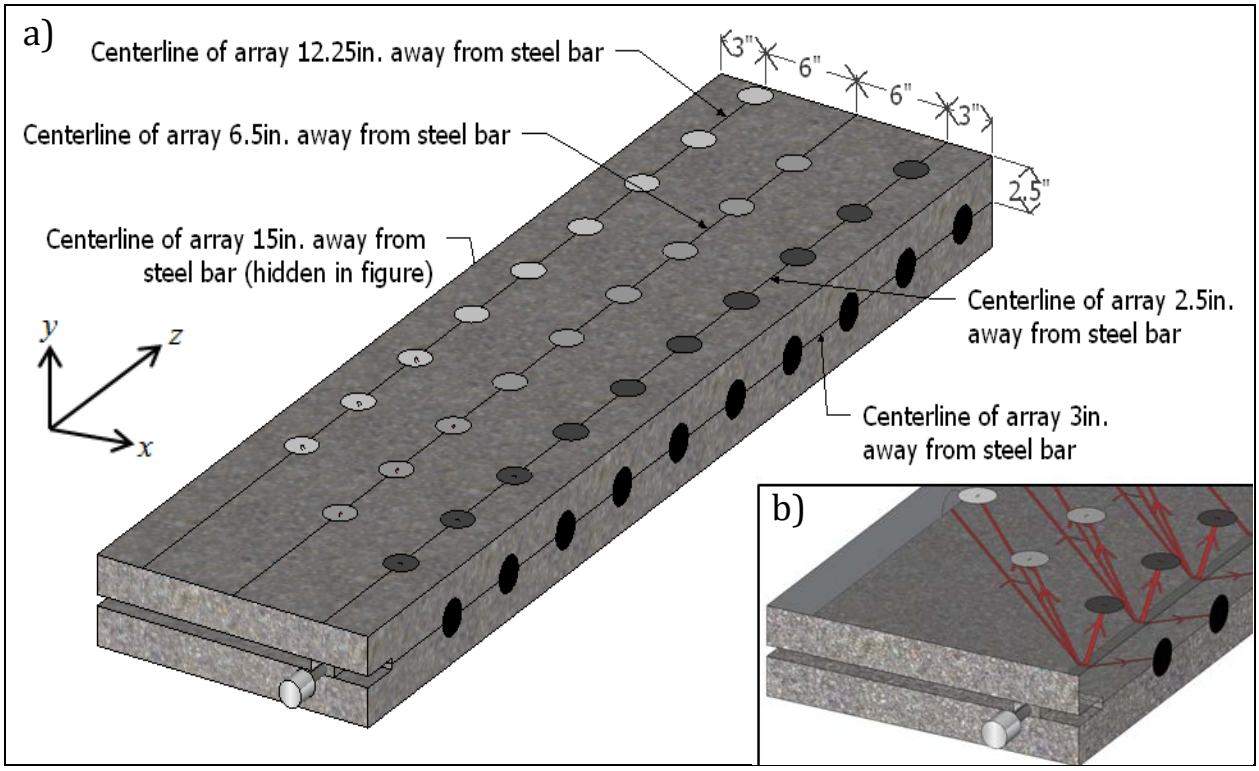

Figure 12. a) Arrays of transducer locations parallel to steel bar and b) path of leaked waves from points along steel bar to transducer locations.

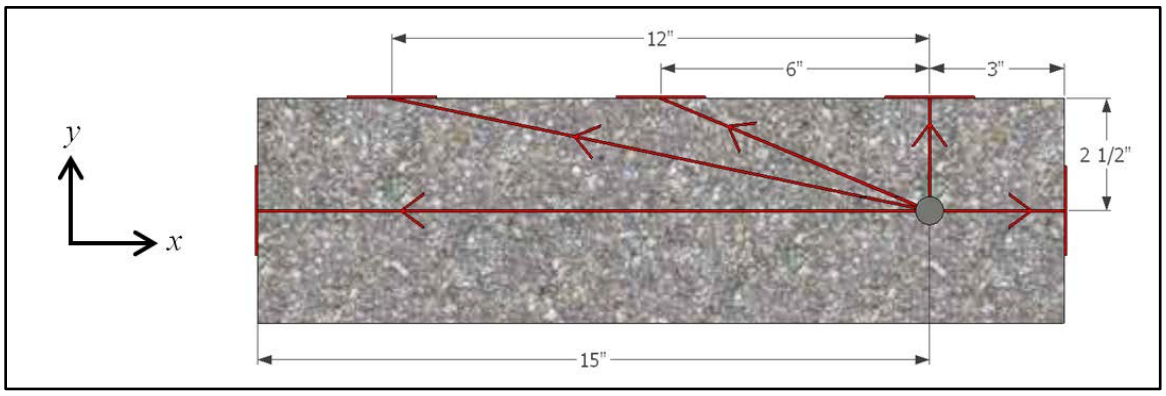

Figure 13. Paths of leaked waves from steel bar to array locations (x-y plane) (Specimen set 2).

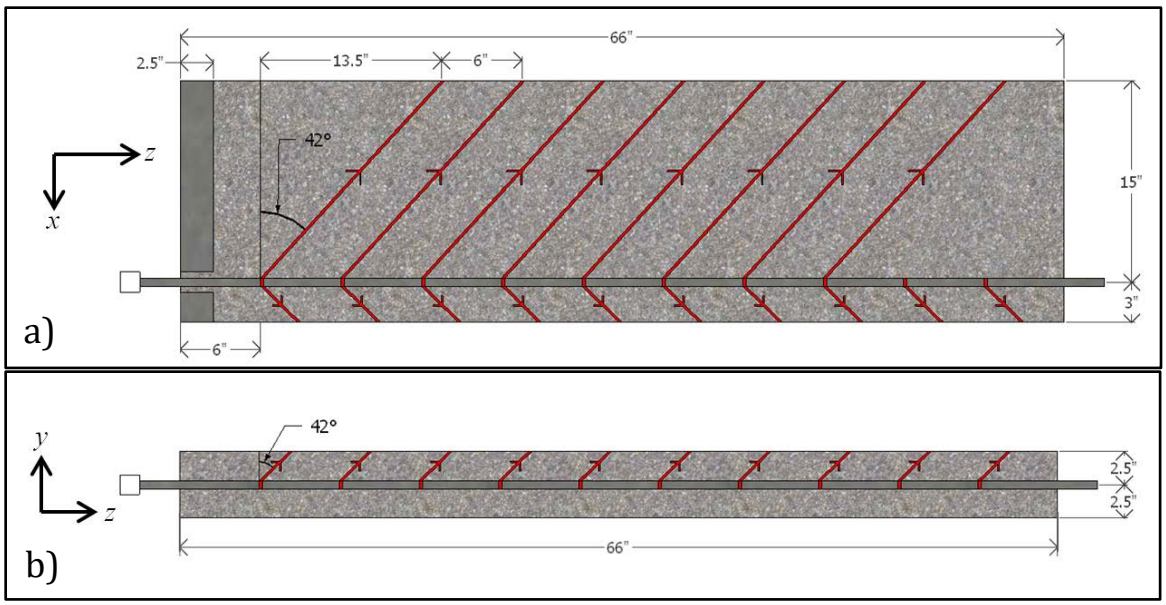

Figure 14. Cross sections at steel bar location in a) x-z plane, and b) y-z plane (Specimen set 2).

4. Discussion of Results

This experimental program comprised of two sets of specimens. The first set of specimens examined the effectiveness of different testing arrangements (existing and proposed) to identify onset of delamination using amplitude and velocity measurements. Specimen set one monitored a delamination of consistent length, allowing all measurements to be correlated with just the width of the delamination. The second set of specimens focused on the proposed testing novel arrangement, UGWL, looking at the inspection area limits of the method. Specimen set two monitored larger specimens with delaminations occurring only in a section of the specimen; meaning ultrasonic readings were collected monitoring delaminations with varying lengths and widths.

4.1. Specimen set 1

4.1.1. Existing UT set-ups: UGW, UPV-Direct and UPV-Indirect

Figures 15 to 17 present sample time and frequency domain plots using UGW, UPV direct and UPV indirect, test arrangements that have been either previously used in research or have been standardized for practice. Time domain plots relate to velocity measurements and the frequency domain allows amplitude measurements.

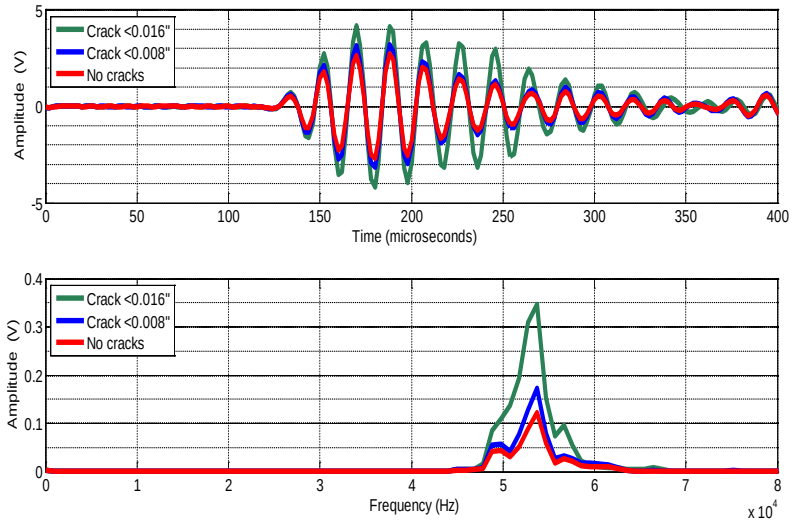

UGW	Velocity (ft/s)	Change from no crack (%)
No Crack	19460	-
<0.008”	19520	+0.31
<0.016”	19520	+0.31

UGW	Amplitude (V)	Change from no crack (%)
No Crack	0.120	-
<0.008”	0.165	+37.5
<0.016”	0.345	+187.5

*Conversion factor: *0.2mm = 0.008”*

Figure 15. UGW *(Figure 5a):* Transducers located at ends of rebar

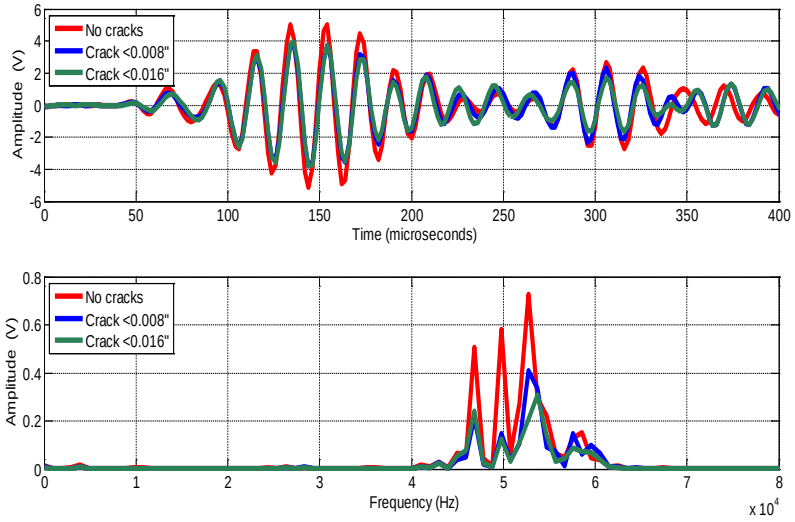

UPV Direct	Velocity (ft/s)	Change from no crack (%)
No Crack	10953	
<0.008”	10891	-0.57
<0.016”	10676	-2.5

UPV Direct	Amplitude (V)	Change from no crack (%)
No Crack	0.730	
<0.008”	0.405	-44.5
<0.016”	0.305	-58.2

*Conversion factor: *0.2mm = 0.008”*

Figure 16. UPV *(Figure 5b):* Direct (Gain 10)

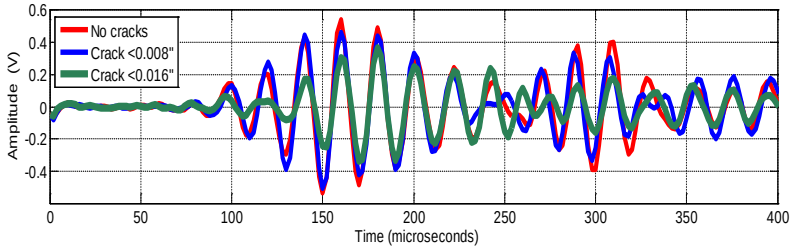

UPV Indirect	Velocity (ft/s)	Change from no crack (%)
No Crack	11261	
<0.008”	11261	0
<0.016”	10874	-3.4

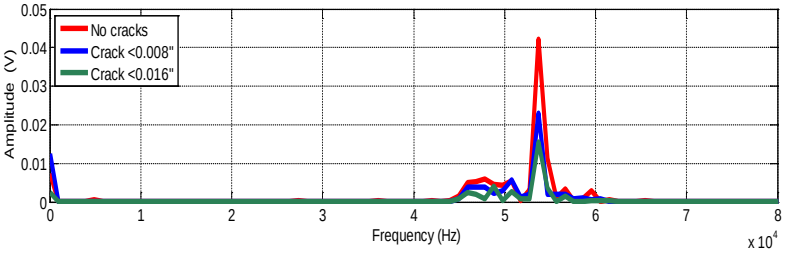

UPV Indirect	Amplitude (V)	Change from no crack (%)
No Crack	0.042	
<0.008”	0.023	-45.2
<0.016”	0.015	-64.3

*Conversion factor: *0.2mm = 0.008”*

Figure 17. UPV *(Figure 5c)*: Indirect (Gain 10)

Tables 3-5 summarize the changes in amplitude and velocity measurements collected from existing UT arrangements with respect to the measured incremental changes applied by the mechanical separation device, or the maximum (measured) delamination width size. The tables only summarize the *changes* in readings during the early stages of delamination formation (i.e. 0.008” and 0.016”).

Table 3 – UGW *(Figure 5a)*: Summary of amplitude and velocity changes

UGW *(3 transducers monitored)*		
Maximum delamination width	**Change of Amplitude (%) ± Confidence Interval**	**Change of Velocity (%) ± Confidence Interval**
<0.008”	40.3 ± 7.8	0.16 ± 0.17
<0.016”	127 ± 60	0.18 ± 0.18

Table 4 – UPV Direct *(Figure 5b)*: Summary of amplitude and velocity changes

UPV Direct *(3 transducers monitored)*		
Maximum delamination width	**Change of Amplitude (%) ± Confidence Interval**	**Change of Velocity (%) ± Confidence Interval**
<0.008”	-32.7 ± 17.8	-0.41 ± 0.57
<0.016”	-46.7 ± 21.4	-1.23 ± 1.74

Table 5 – UPV Indirect *(Figure 5c)*: Summary of amplitude and velocity changes

UPV Indirect *(3 transducers monitored)*		
Maximum delamination width	**Change of Amplitude (%) ± Confidence Interval**	**Change of Velocity (%) ± Confidence Interval**
<0.008”	-39.3 ± 9.9	-0.67 ± 0.65
<0.016”	-56.7 ± 11.8	-5.67 ± 8.34

The results shown in Table 3, 4 and 5 demonstrate that velocity measurements were at least ten times less sensitive than amplitude measurements for UGW, direct and indirect UPV test arrangements. The changes in amplitude measurements with respect to delamination width demonstrated consistency regardless of set-up or path length. However, only the UGW method amongst these can state the delamination actually occurs between the steel bar and concrete. The velocity-based arrangements can only conclude that a delamination developed somewhere in the specimen.

4.1.2. Proposed novel UT method: UGW Leakage (UGWL)

Figure 18 illustrates the different scenarios that are examined with the proposed novel UGWL test set-up. The presence of one delamination brings up two scenarios: a) when the delamination disrupts the path of the leaked bulk waves to the sensor (sample of results shown in Figure 19) and b) the delamination does not disrupt the path of the leaked bulk waves to the sensor (sample of result shown in Figure 20).

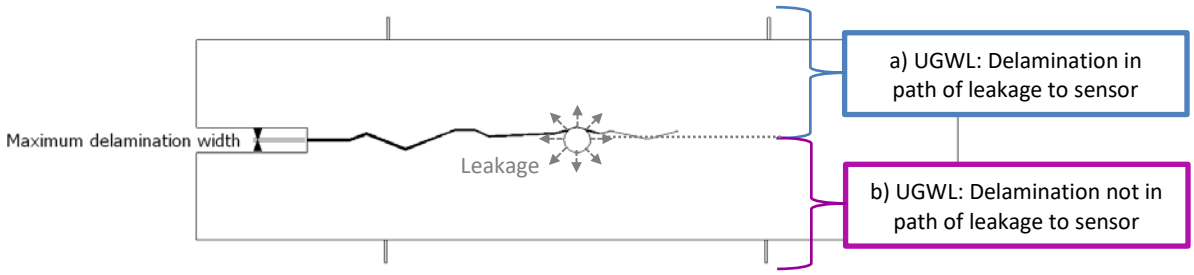

Figure 18. Ultrasonic Guided Wave Leakage (UGWL) measurement scenarios

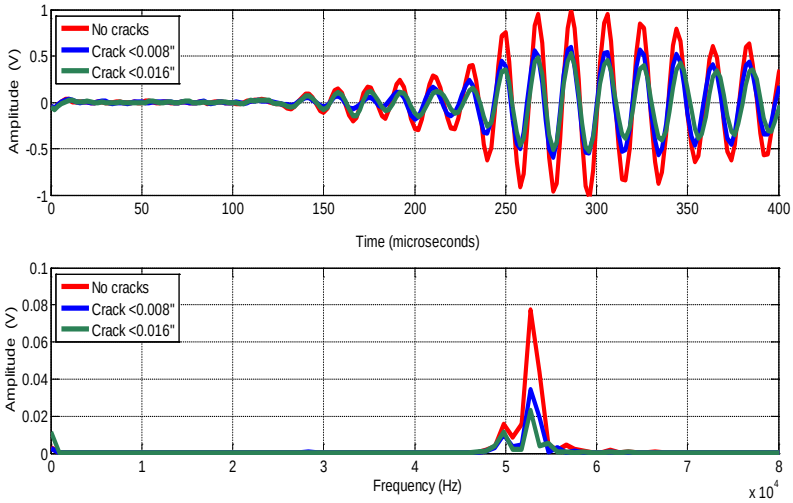

UGWL	Velocity (ft/s)	Change from no crack (%)
No Crack	13211	-
<0.008”	13089	-0.92
<0.016”	13089	-0.92

UGWL	Amplitude (V)	Change from no crack (%)
No Crack	0.076	-
<0.008”	0.033	-56.5
<0.016”	0.022	-71.1

*Conversion factor: *0.2mm = 0.008”*

Figure 19. UGWL *(Figure 5d and 18a)*: Delamination in path of leakage – Transducer (Gain 10)

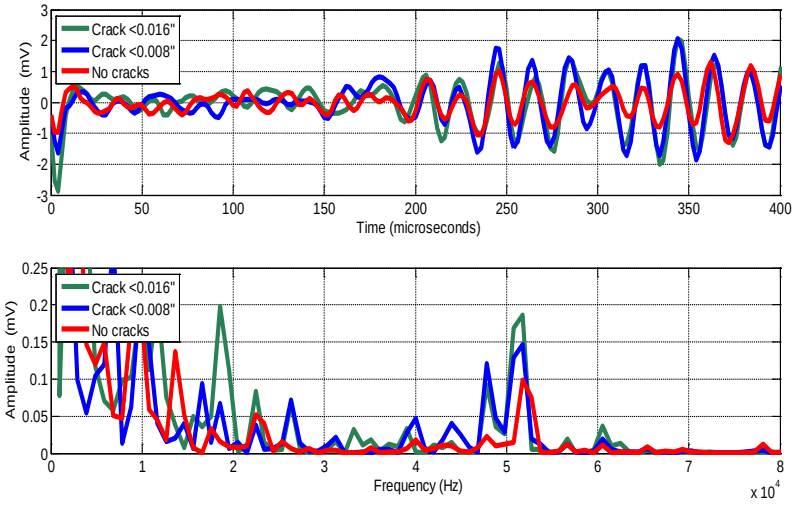

UGWL	Velocity (ft/s)	Change from no crack (%)
No Crack	12051	
<0.008”	12056	+0.04
<0.016”	12060	+0.07

UGWL	Amplitude (mV)	Change from no crack (%)
No Crack	0.099	
<0.008”	0.148	+49.5
<0.016”	0.18	+81.8

*Conversion factor: *0.2mm = 0.008”*

Figure 20. UGWL *(Figure 5d and 18b)*: Delamination not in path of leakage – Pinducer (60dB & Gain 1000)

Figures 19 and 20 show sample results of scenarios shown in Figure 18a and 18b, respectively. Table 6 summarizes the results of all sensors (2 inch diameter transducers and pinducers) , which monitored the signals that had a delamination disrupt the path of leaked waves and demonstrates that regardless of the transducer used or path length, the change in amplitude with respect to delamination width is consistent.

Table 7 summarizes the results of the sensors that monitored signals that were not disrupted by the delamination, sample of results shown Figure 20. Table 7 shows that when a delamination began to occur between the steel and concrete, but did not interfere with the path of the leaked bulk waves to the sensor, the amplitude of the leaked bulk waves detected increased.

Table 6 – UGWL *(Figure 5d and 18a)*: Summary of amplitude and velocity changes

UGWL: Delamination in path of leakage to sensor *(10 transducers monitored)*		
Maximum delamination width	**Change of Amplitude (%) ± Confidence Interval**	**Change of Velocity (%) ± Confidence Interval**
<0.008”	-51.5 ± 8.2	-1.6 ± 1.7
<0.016”	-71.7 ± 5.2	-5.9 ± 4.7

Table 7 –UGWL *(Figure 5d and 18b)*: Summary of amplitude and velocity changes

UGWL: Delamination not in path of leakage to sensor *(4 transducers monitored)*		
Maximum delamination width	**Change of Amplitude (%) ± Confidence Interval**	**Change of Velocity (%) ± Confidence Interval**
<0.008”	55.1 ± 4.3	0.03 ± 0.03
<0.016”	84.4 ± 3.3	0.04 ± 0.02

Figure 21 and Figure 22 plot the calculated data using the damage indices, the average changes, and the confidence intervals of the changes in amplitude and velocity measurements (shown in Tables 6-7) with respect to maximum (measured) delamination width for the UGWL test set-up scenarios shown in Figure 18.

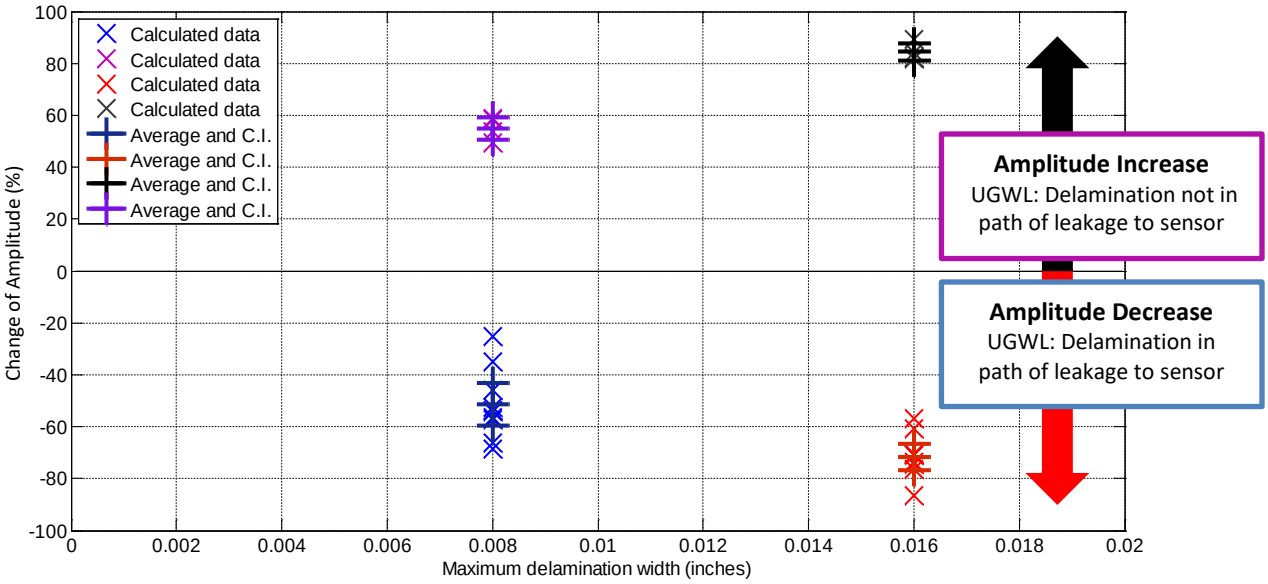

Figure 21. UGWL set-up (Figure 18): Percent change of amplitude due to onset of delamination

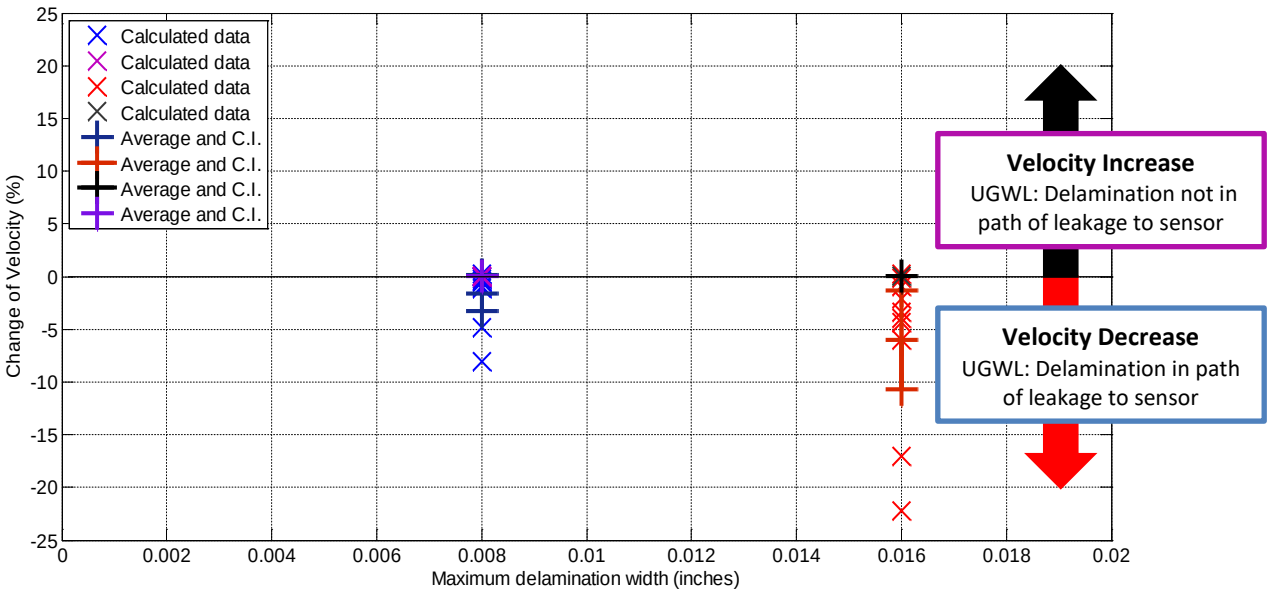

Figure 22. UGWL set-up (Figure 18): Percent change of velocity due to onset of delamination

Figure 21 illustrates that there are correlations between delamination width and leakage amplitude. However, several of the collected data points fall significantly outside of the confidence interval upper and lower bounds. Figure 22 plots the velocity based results from the set-up monitoring the UGW leakage (Figure 18) and clearly shows that velocity measurements were not very sensitive to delaminations less than 0.016". There were some substantial changes in velocity when the maximum delamination width reached 0.016"; however, changes ranging from 0-22% demonstrate that velocity measurements are not sensitive enough to consistently identify delaminations 0.016" wide. Several of the calculated data points for velocity were also significantly outside the confidence intervals.

The delamination width that measurements have been correlated with thus far has been the maximum delamination width in the specimen (separation at the mechanical device). Figure 23a shows that the delamination appears to decrease linearly to the effective pivot point, the end of the specimen, likely due to weak bond caused by casting the specimen in layers. This linear estimation is illustrated in Figure 23b. If the delamination width decreases along the length of the specimen, as shown in Figure 23b, the delamination between concrete and rebar would also differ along its circumference. The variation of delamination widths along the circumference could theoretically explain why some calculated data points were significantly outside the confidence intervals as this would influence the leakage detected by the sensors. Estimations of the delamination around the circumference of the rebar with respect to an incremental change of 0.008" are shown in Figure 23c.

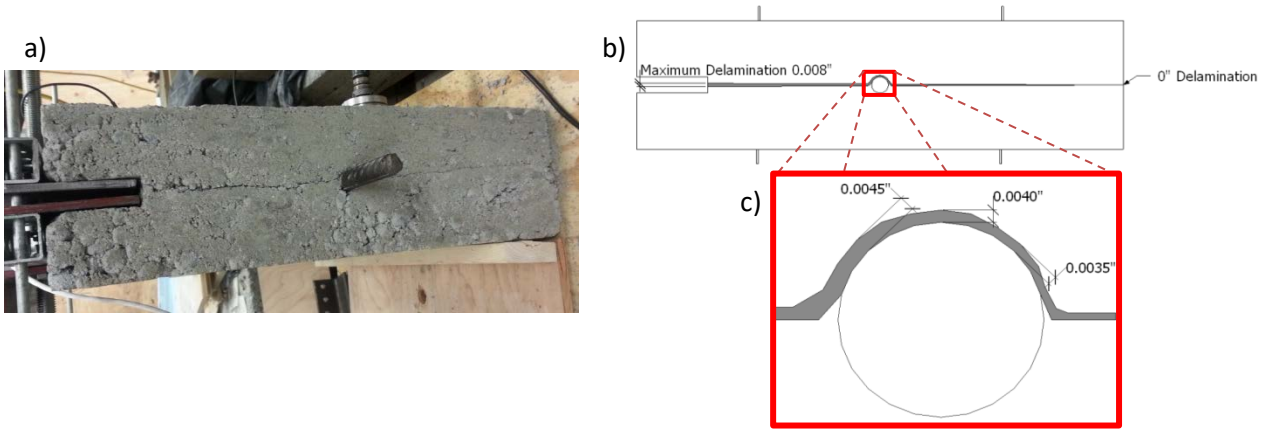

Figure 23. Estimation of delamination between rebar and concrete (Specimen set 1)

Figure 24 plots the average and confidence intervals of data collected using the UGW leakage set-up against the estimated delamination widths. The grey band gives the estimated correlation between the changes of amplitude and delamination width. The boundaries of the grey band are the fitted logarithmic curves of the lower and upper confidence intervals. The yellow band gives the estimated correlation between the changes of velocity and delamination width. The boundaries of the yellow band are the fitted 2nd order polynomial curves of the lower and upper confidence intervals. The fitted curves are shown as dashed lines in Figure 24.

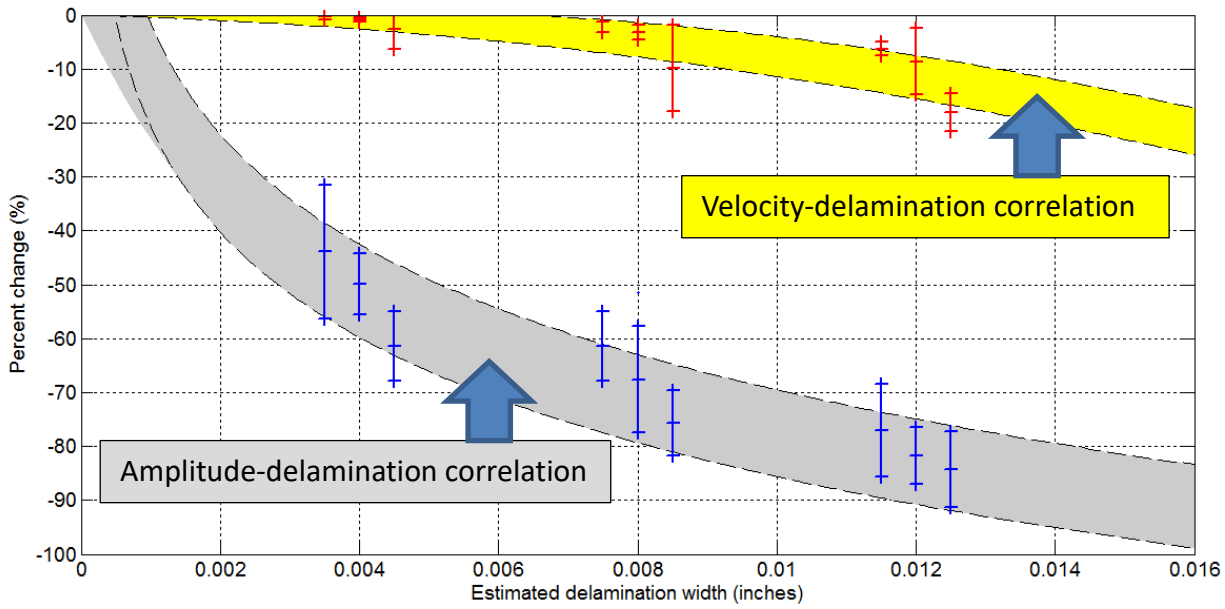

Figure 24. Percent change of amplitude and velocity of UGWL (*Figure 5d and 18a*) due to onset of *estimated* delamination (Specimen set 1)

The boundaries for both bands were determined only using the confidence intervals of data collected from the 0.008" and 0.016" measured increments, which provided the data at the 0.0035"-0.0045" and 0.0075"-0.0085" delamination widths, respectively. Data collected from the 0.024" increment, which provided the data at the 0.0115"-0.0125" delamination widths, was added to Figure 24 to illustrate how well the data fit the estimation bands determined. It was found that amongst all the calculated data points used to develop Figure 24, none of them fell more than 5% from a confidence interval and that 80% of them were within the bands.

4.2. Specimen set 2

Specimen set 2 examined limitations of the UGWL arrangement. The results are presented and discussed in four subsections that align with the objectives set out for this specimen set. The first shows a short study verifying the leakage angle prior to introducing delamination to the specimens. The second presents the correlations found from an array of amplitude readings with the growth in length of a delamination. The third subsection discusses the distance limitations of the UGWL approach by examining the attenuation coefficients of the guided wave and the leakage amplitude, and how these are influenced by the presence of a delamination. The fourth subsection presents the correlations of the amplitude and velocity readings collected by an individual sensor in the array with delamination length and width.

1) Verification of leakage type.

To verify the type of leakage detected, specimens were tested before damage was introduced to the specimens and readings were compared to theoretical values. For the verification study, the locations along the arrays were not determined with respect to the theoretical leakage angle. Both velocity and amplitude measurements were analyzed to verify and validate the use of theoretical longitudinal leakage angle as the propagation path. Tables 8 and 9 show how the theoretical arrival times of leaked longitudinal and shear bulk waves compared to the actual arrival times collected from sensor locations along arrays 6.5 and 12.25 inches away from the steel bar, respectively. In Tables 8 and 9, the theoretical arrival times of the longitudinal (P-wave) and shear (S-wave) waves are highlighted in blue and orange, respectively, and the actual

times are highlighted blue or orange depending on what theoretical time it correlated with. If white, the arrival time was in between both theoretical times.

Table 8- Theoretical and actual arrival times of leaked waves – Array 6.5 in. away from bar

Array 6.5in. away from bar								
Location on concrete in z-direction	6	12	24	30	36	48	54	60
Theoretical Time of P-wave (µs)	69.5	95.6	147.7	173.7	199.8	251.9	277.9	304.0
Theoretical Time of S-wave (µs)	100.7	126.8	178.9	204.9	231.0	283.1	309.1	335.2
Actual Time (µs)	73	102	147	176	204	249	290	335
Figure (Appendix A)	A.1	A.2	A.3	A.4	A.5	A.6	A.7	A.8

Table 9-Theoretical and actual arrival times of leaked waves – Array 12.25 in. away from bar

Array 12.25in. away from bar							
Location on concrete in z-direction	6	18	24	30	36	48	60
Theoretical Time of P-wave (µs)	96.5	148.6	174.6	200.7	226.7	278.8	331.0
Theoretical Time of S-wave (µs)	155.3	207.4	233.5	259.5	285.6	337.7	389.8
Actual Time (µs)	132	143	172	192	223	283	333
Figure (Appendix B)	B.1	B.2	B.3	B.4	B.5	B.6	B.7

As can be seen in Tables 8 and 9, the majority of the actual arrival times correlated well with the theoretical arrival time of the leaked longitudinal waves. The arrival times did not correlate with theoretical longitudinal arrival time when the sensor was located prior to the point that the 42° angle (6 inch point along array 12.25 inches away from the bar) or farther. Further down the array, the arrival time eventually correlated with the arrival time of the leaked shear

waves. This suggests that both longitudinal and shear waves leak out from the waveguide, but the amplitude of the shear wave is greater. This would mean that the leaked longitudinal bulk waves would attenuate before the leaked shear waves do, which agrees with what was observed and shown in Table 8.

Amplitude measurements of the leakage would be influenced by the amplitude of the guided wave at the point in which the bulk wave leaked from. The guided wave propagating through the embedded steel bar would attenuate, and the attenuation coefficient of the guided wave in the undamaged specimens could be calculated using Equation 6.The average attenuation coefficient of the embedded guided wave in the undamaged specimens in set 2 was 0.052 Np/in. Theoretically, the attenuation of the leaked waves in the direction of the guided wave (z-direction) would correlate to the attenuation of the guided wave itself. Figure 25 shows amplitudes collected from an array 15 inches away from the bar in both delamination specimens in set 2 prior to damage. These showed amplitudes only beginning to exponentially decrease just past 16 inches in the axial direction (z-direction) (Figure 25), which is the sum of the 13.5 inches caused by leakage angle of the longitudinal bulk waves and the 2.5 inches disruption caused by the slot for the separating device (Figure 26). The curve drawn in Figure 25 is the fitted exponential curve for points along the steel bar examined beyond 16 inches.

The attenuation coefficient of the leaked bulk waves in the z-direction, which was 0.052 Np/in, was determined by the fitted exponential curve in Figure 25 and matched the attenuation coefficient of the guided wave.

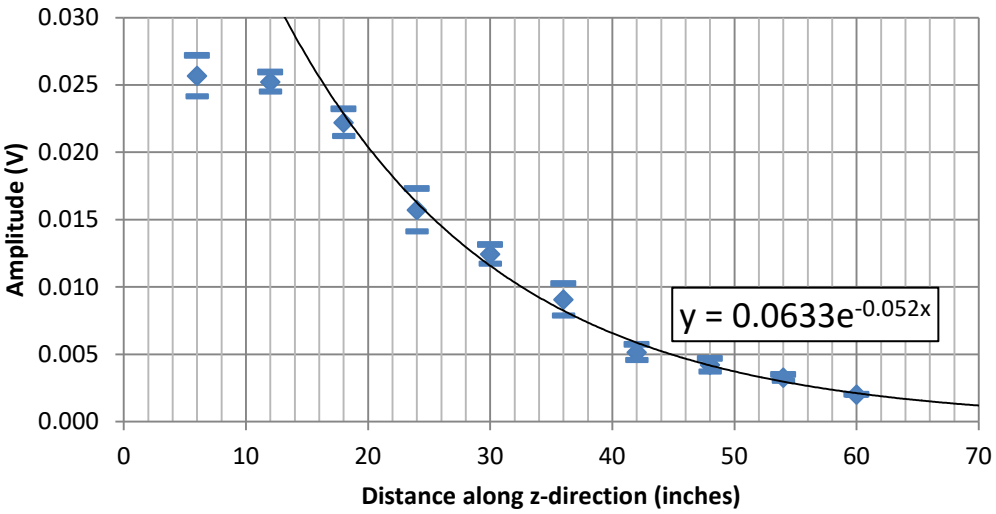

Figure 25- Amplitudes of leakage along edge parallel to steel bar 15 inches away.

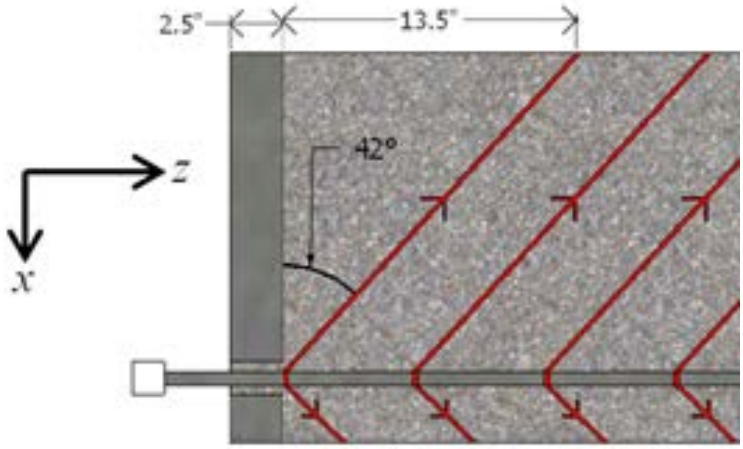

Figure 26 – Path of first leaked longitudinal wave to where exponential decay begins.

These findings verified that both types of leakage occurred in this guided wave system, and that the calculated angles correlate well with angles of leakage that occurred in the experimental study. Also, although the leaked shear bulk waves likely had higher amplitudes, the collected measurements of arrival time and the correlation of amplitudes in the frequency domain were controlled by the leakage angle of the longitudinal bulk waves. Since the velocity and leakage

angle of the leaked longitudinal bulk waves were greater than that of the leaked shear waves, measurements and correlations would be more inclusive of both types of leakage if the path used to analyze data was determined by the leakage angle of the longitudinal bulk waves.

2) Correlation of amplitude readings from array of sensors with delamination length.

Two concrete specimens were cast, specimen A and B. The delamination in specimen A, created using the mechanical device, developed to be a 14 inch long crack along the level of the reinforcing steel bar. Specimen B only developed a 6.5 inch long crack along the level of the embedded steel bar. Figure 27 shows some of the stages of crack development of specimen A.

Figures 28, 30, and 31 show how the length of the delamination that developed in specimen A influenced the amplitudes of different arrays of transducer locations. Figure 28 plots the change in amplitude readings of the array of transducers located 2.5 inches away from the steel bar. The delamination that developed between the steel bar and concrete eventually interrupted the path of the leaked waves to the transducers in this array monitoring the 6 and 12 inch points along the steel bar. The amplitude of leakage detected by these transducers decreased when the delamination reached those points along the bar. In addition, the transducers located to monitor points beyond the delamination length consistently saw increases in amplitude readings in specimen A. Figure 29 depicts the orientation of the delamination with respect to the path of the leaked waves to these transducers (array 2.5 inches away). The combination of behaviors due to the onset and development of a

delamination allowed the location of the delamination to be estimated since the peak amplitude of the array would occur soon after the delamination.

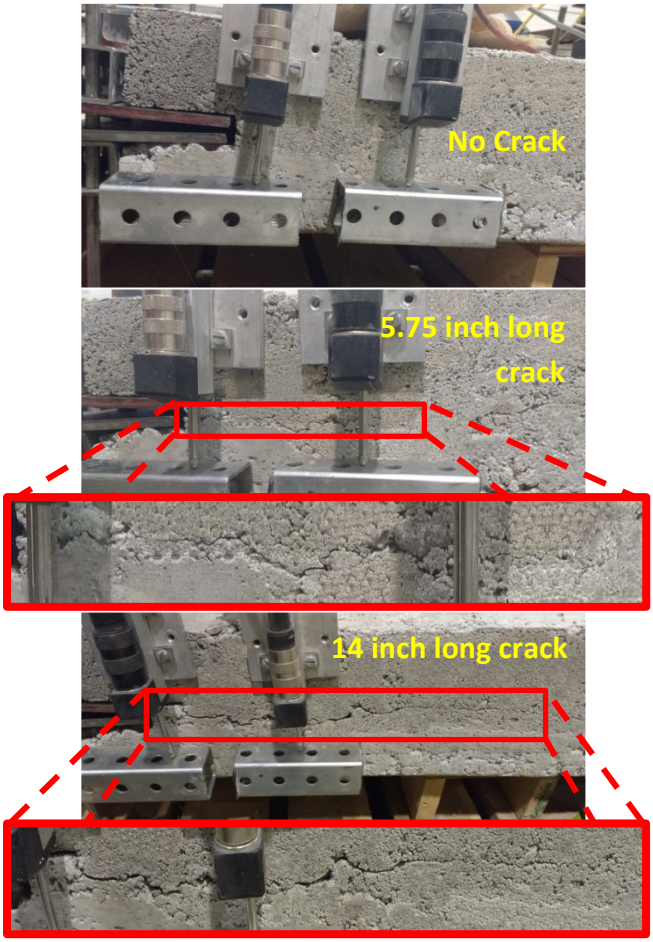

Figure 27. 14 inch long delamination in Specimen A. (Specimen set 2)

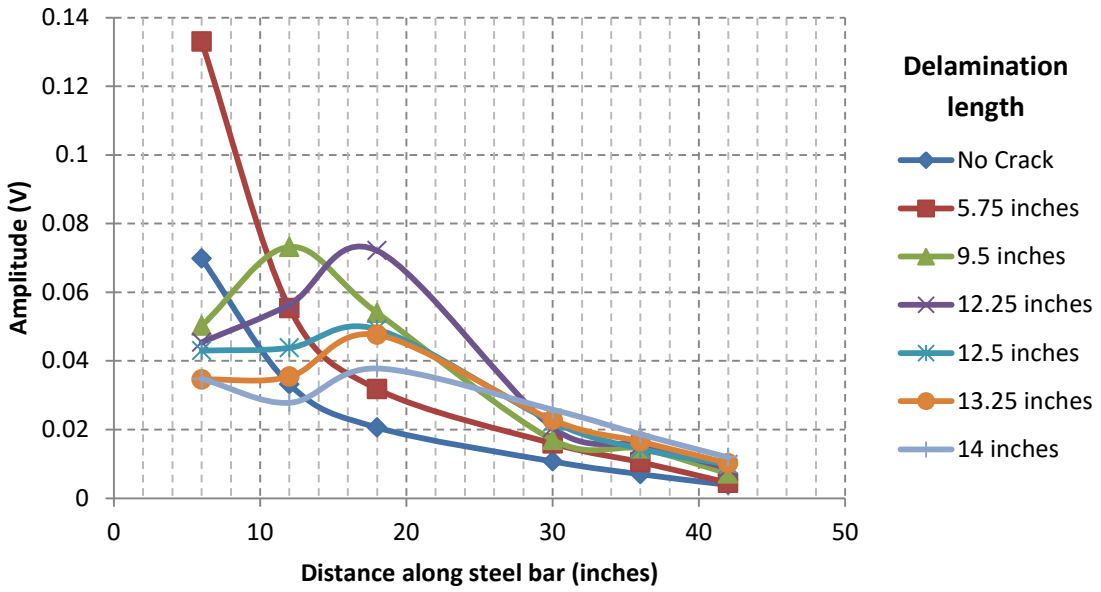

Figure 28. Amplitude with respect to delamination length monitored by the array 2.5 inches away from steel bar.

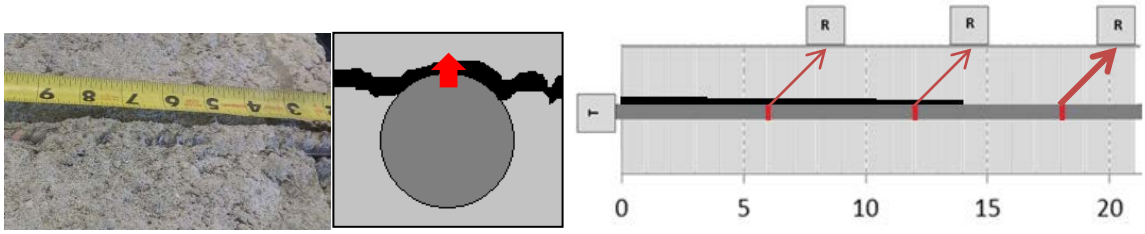

Figure 29. Orientation of delamination with respect to path of leaked waves monitored by transducers in array 2.5 inches from steel bar.

Given that the delamination between the steel and concrete formed along the top of the reinforcing steel bar, the array of sensor locations along sides of the steel bar (the arrays 3 and 15 inches away from steel bar) were expected to have similar correlations to one another as the delamination did not appear to interrupt the path of leaked waves to either array. Figures 30

and 31 show how the amplitudes of signals monitored by arrays 3 and 15 inches away from steel bar, respectively, changed as delamination grew. In Figure 31, the array of sensors located on the parallel edge 15 inches away from the steel bar consistently saw increases in amplitude throughout the array as the delamination grew wider and longer. However, the array of sensors located 3 inches away did not. The sensor monitoring the 12 inch location along the steel bar saw decreases once the delamination reached 12.25 inches long, shown circled in Figure 30. The specimen was opened up along the delamination after testing and at the 12 inch point along the steel bar it was found that the side facing toward the array 3 inches away from the steel bar had delaminated from the concrete, as shown in Figure 32.

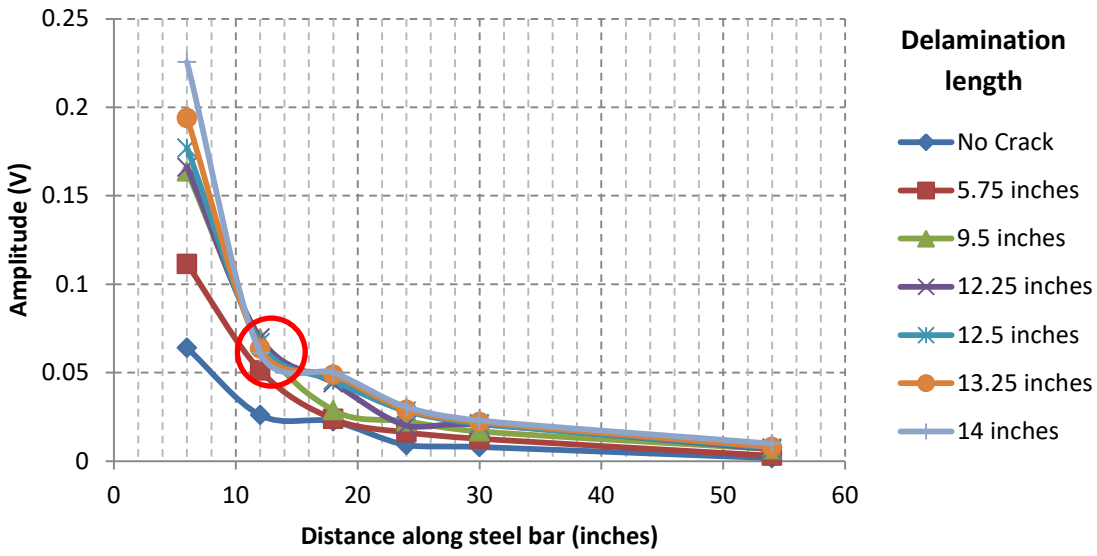

Figure 30. Amplitude with respect to delamination length monitored by the array 3 inches away from steel bar.

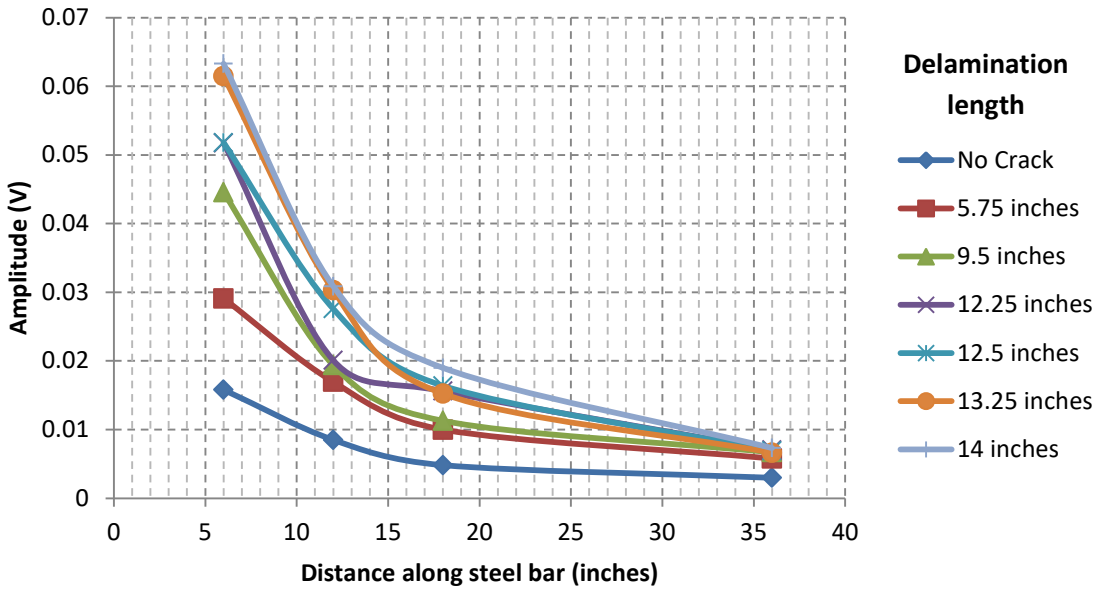

Figure 31. Amplitude with respect to delamination length monitored by the array 15 inches away from steel bar.

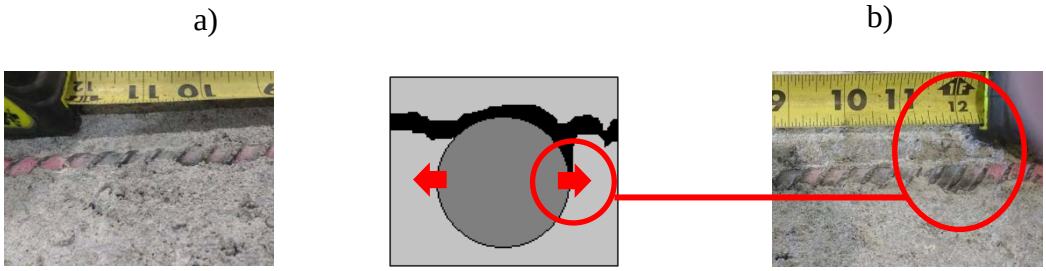

Figure 32. The delamination at the 12 inch point along the steel bar: a) side facing array 15 inches away, and b) side facing array 3 inches away.

Specimen B also demonstrated that amplitude readings decrease once the delamination interrupted the leakage path, and a substantial increase is found right after the delamination region. Specimen B demonstrated that this arrangement can be effective in identifying the

presence of a delamination 2 inches long and only 0.002 inches wide (Figure 33) while increases in amplitude could be found four feet away from the delamination.

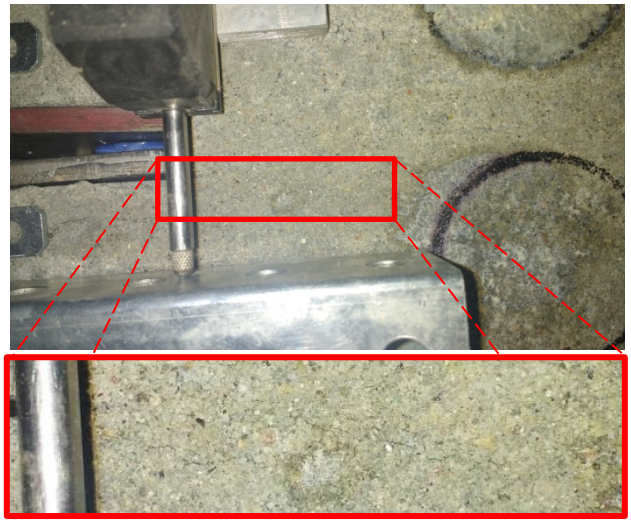

Figure 33. 2 inches long and 0.002 inches wide delamination in Specimen B

However, specimen B demonstrated that not only does the presence of a delamination allow for more energy to be leaked out beyond the delamination, but that the attenuation coefficient of the leakage in the z-direction (therefore likely the guided wave as well) increases. This can be observed in the results of specimen A as well. However, in specimen B, the increase of attenuation coefficient was substantial enough to cause the amplitude readings at monitoring locations beyond 42 inches (from end of specimen where crack is created) to decrease rather than increase. These readings can be seen in Figures 34 and 35. Further discussion on the increase of attenuation coefficient is presented in the following subsection.

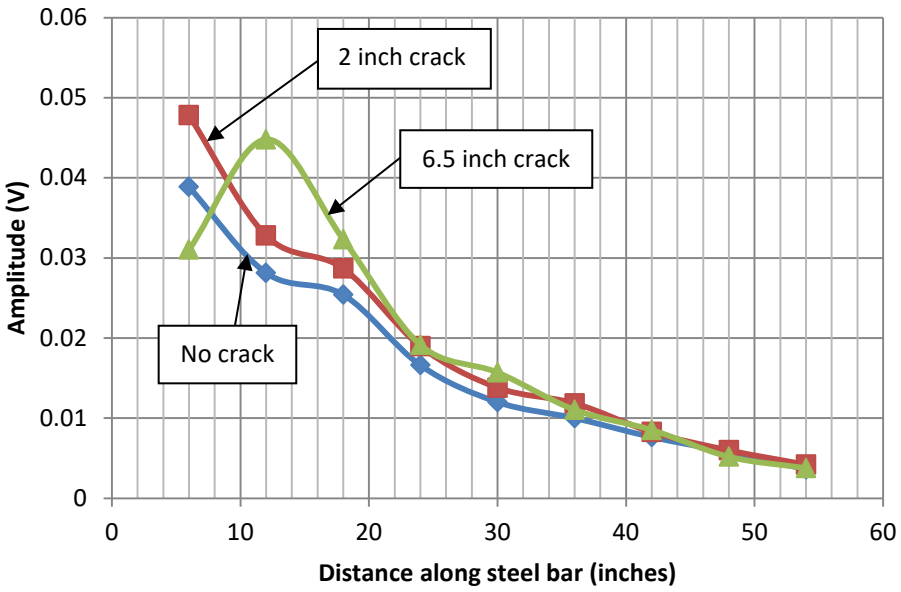

Figure 34. Correlation between amplitude and delamination length of Specimen B for array located 6.5 inches from steel bar.

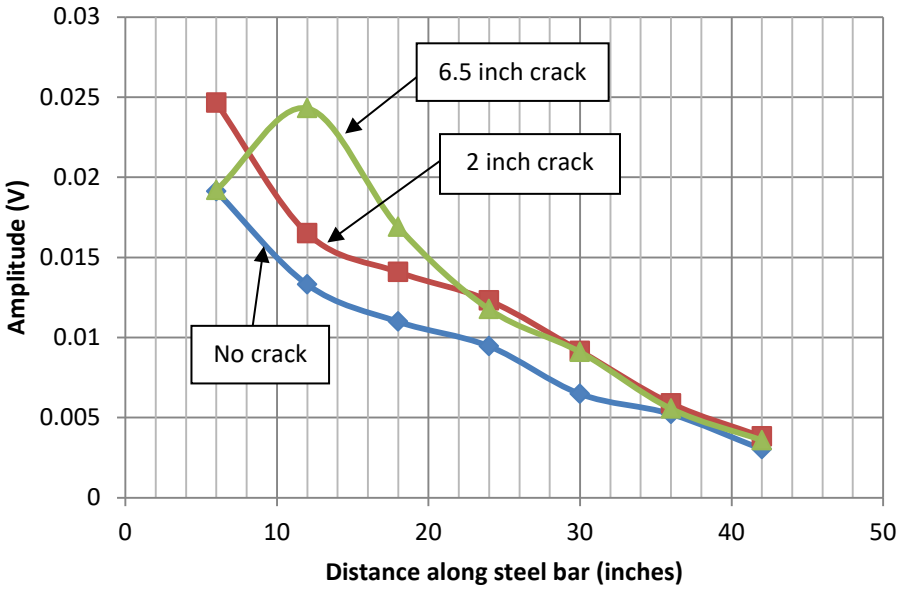

Figure 35. Correlation between amplitude and delamination length of Specimen B for array located 12.25 inches from steel bar.

3) Propagation limits and the influence of delamination growth on attenuation coefficient

The attenuation coefficients of the guided wave and the leaked waves were examined. The attenuation of the leaked bulk waves was examined in both the direction of the leakage propagation and in the z-direction. The attenuation coefficients were determined from the fitted exponential curves for the averages of amplitude readings.

a) Attenuation of guided wave and leakage in the z-direction

Before any delamination was created, it was the found that the attenuation coefficient of the leakage in the z-direction was around the same as the attenuation coefficient of the guided wave in areas without high levels of reflections, as can be seen in Figure 36 and Table 10. Arrays 2.5 and 3 inches away from the steel bar had significantly greater attenuation coefficients than arrays 6.5, 12.25 and 15 inches away from the steel bar, shown in the fitted exponential curves to the average amplitudes collected. The authors believe this is likely due to surrounding boundaries being much closer, causing high levels of reflected waves to be detected early, which gradually attenuates in the concrete further down in the z-direction. The arrays located at further distances from the steel bar demonstrated attenuation coefficients similar to that of the guided wave, which was determined by measurements collected at the end of the steel bar.

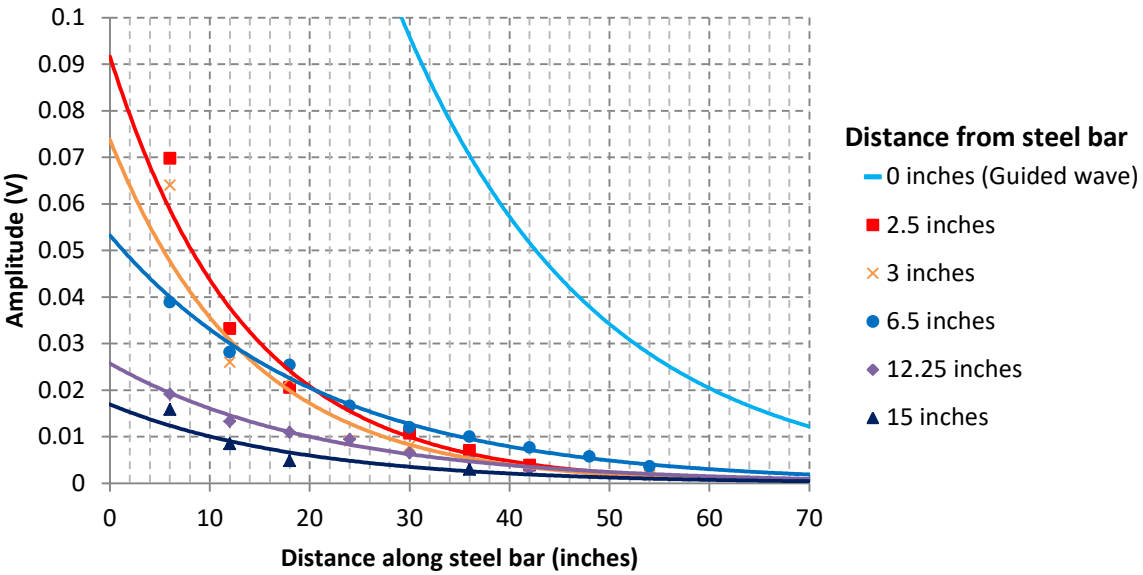

Figure 36. Attenuation of sensor arrays (and guided wave) prior to delamination.

Table 10. Attenuation coefficients of arrays prior to delamination

Distance from wave guide (inches)	Fitted exponential curve equation (Figure 36)	Attenuation Coefficient (Np/in)
0 (Guided wave)	$y=0.4500e^{-0.052x}$	0.052
2.5	$y=0.0916e^{-0.074x}$	0.074
3	$y=0.0738e^{-0.073x}$	0.073
6.5	$y=0.0533e^{-0.048x}$	0.048
12.25	$y=0.0170e^{-0.047x}$	0.047
15	$y=0.0257e^{-0.052x}$	0.052

After the delamination was created, it was consistently found that the attenuation coefficient of the leaked waves in the z-direction detected by sensors beyond the delamination length had increased. Examples of this are illustrated for specimen A in Figures 37 and 38, and Table 11, and for specimen B in Figures 39 and 40.

In specimen B, the increase in attenuation coefficient was large enough to cause the amplitudes of some of the further points to decrease rather than increase, as seen in Figures 39 and 40. The authors believe that this increase in attenuation coefficient is due to the stress increase between the concrete and steel bar beyond the delamination point caused by the tension force causing the delamination to grow.

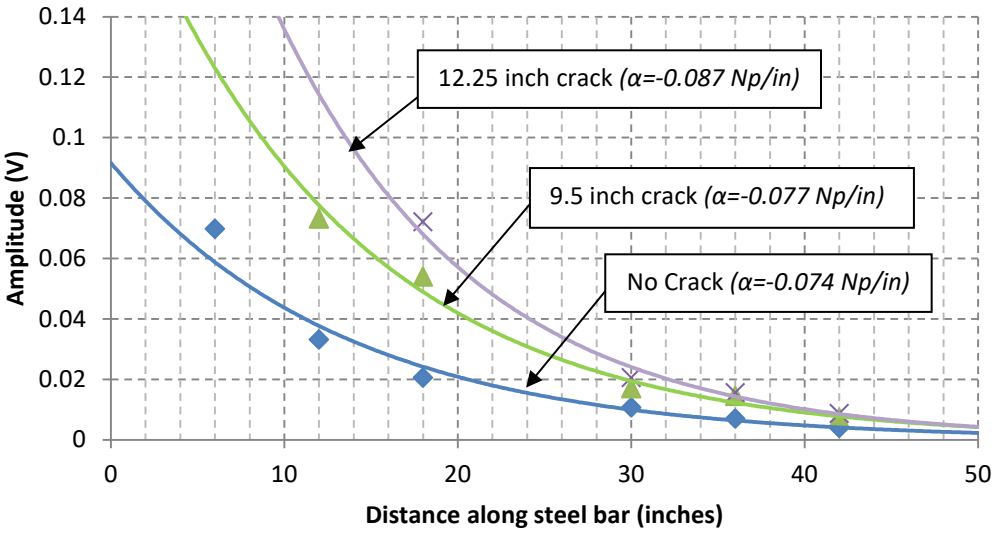

Figure 37. Specimen A: Exponential fitted curves for sensor array 2.5 inches from steel bar for points beyond delamination.

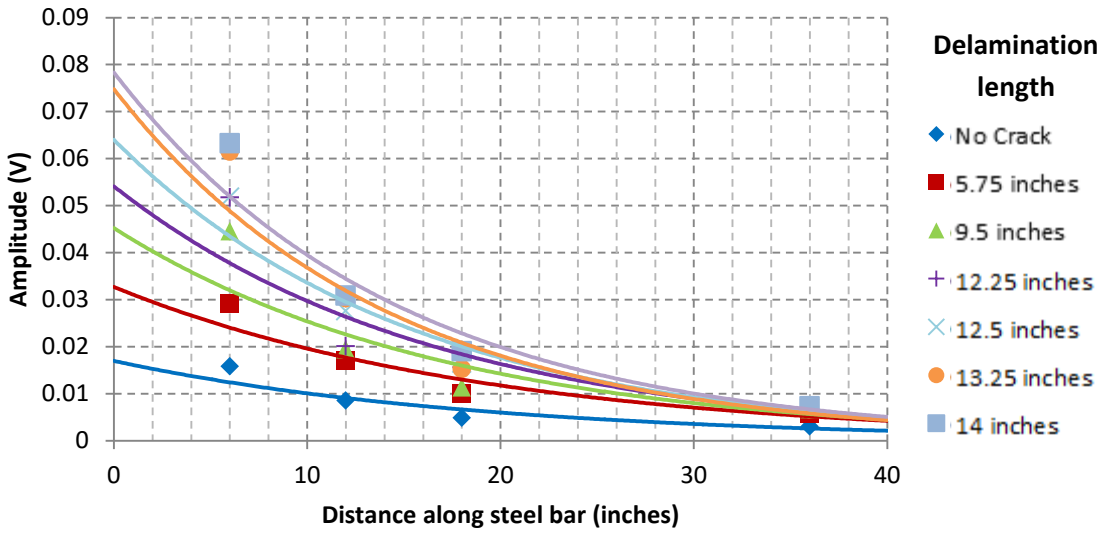

Figure 38. Specimen A: Exponential fitted curves for sensor 15 inches from steel bar for points beyond delamination.

Table 11. Attenuation coefficients determined from curves plotted in Figure 38 (Specimen A).

Delamination length (inches)	Attenuation coefficient (Np/in)
0	0.052
5.75	0.051
9.5	0.058
12.25	0.06
12.5	0.064
13.25	0.071
14	0.069

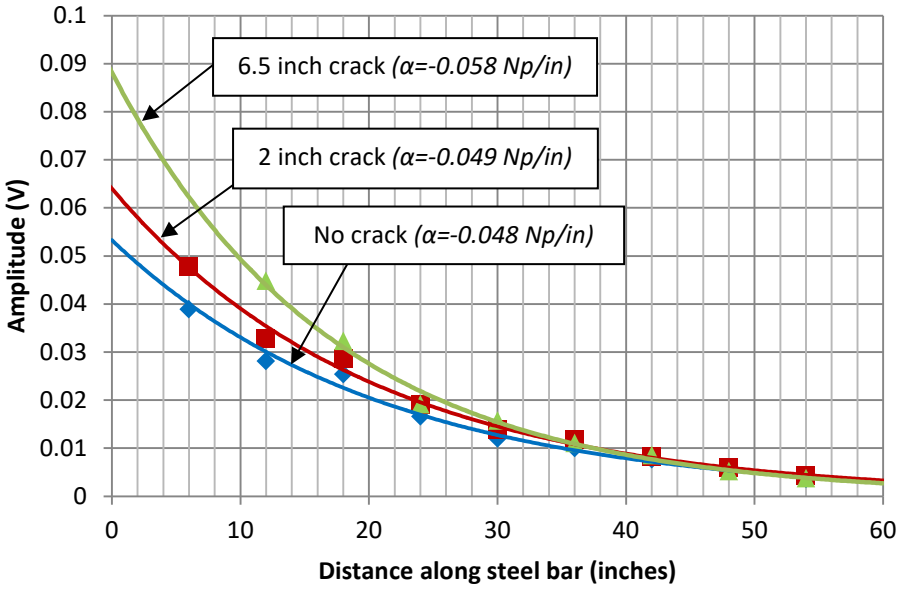

Figure 39. Exponential fitted curves for Figure 34 for points beyond delamination (Specimen B)

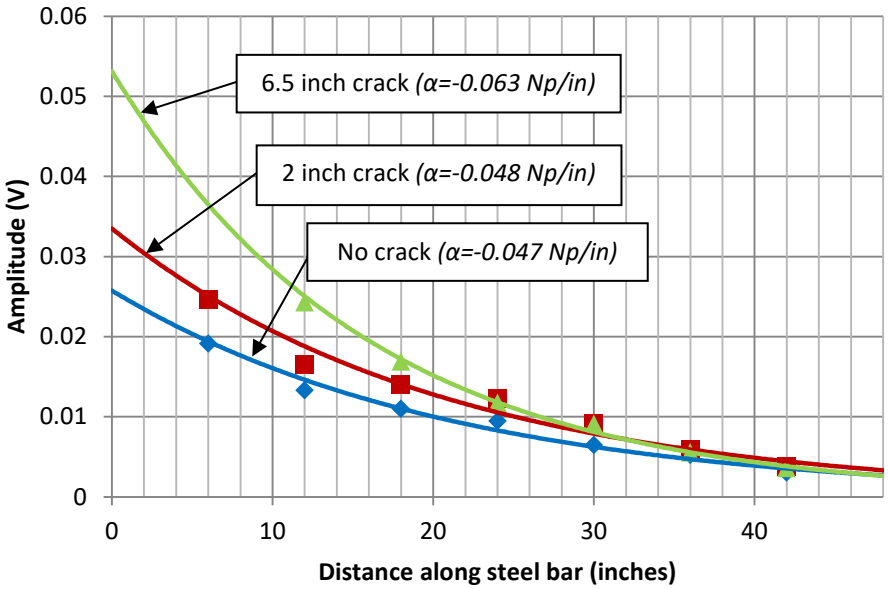

Figure 40. Exponential fitted curves for Figure 35 for points beyond delamination (Specimen B)

b) Attenuation in leakage angle direction

The average attenuation coefficient of the leaked bulk waves traveling through concrete was found to be -7.48Np/m (-0.19Np/in). This average was determined from the attenuation coefficients shown in Table 12. From the amplitudes and the spacing between arrays and bar in the leakage angle direction, the attenuation of the leaked waves could be calculated. Using the average attenuation coefficient of the leaked waves in both the direction of propagation (leakage angle of 42°) and z-direction, the distance limitations of using the UGWL can be determined. Figure 41 illustrates the predicted paths and distances of leakage from the steel bar to reach the amplitude of 0.0014 V, which was the smallest amplitude detected from all arrays in the undamaged specimen. In Figure 41, the x-axis can be visualized as the embedded steel bar with the arrows being the leaked waves from respective points along the steel bar. Figure 41 was developed using the average attenuation coefficient of -0.052 Np/in in the z-direction, which was the attenuation coefficient of the array of sensors at a distance of 15 inches from the bar, and using the average attenuation coefficient of -0.19Np/in in the direction of the leakage propagation. Table 13 shows samples of the furthest signal detected from the specimens. The transducer receiving the signal shown in Table 13 was located at 61.5 inch) in the z-direction from the transmitter (end of steel bar) and 15 inches from the steel bar, shown in Figure 41 by the circle. With respect to the leakage angle, this transducer monitored the 48 inches point along the steel bar. All readings collected, analyzed and presented in specimen set 2 only used a gain of 10 (+20dB) because a gain of 100 (+40dB) or 1000 (+60dB) were generally too strong (i.e. amplitude of signals would max out on the NDE 360 monitor) for locations less than 48 inches from the transmitter. But as Table 13 illustrates, using a higher

gain reduces the amount of noise the signal receives. Therefore, it appears that this method can be used to monitor smaller amplitudes at further distances from the steel bar than what is shown in Figure 41. Assuming an acceptable minimum amplitude of 0.0014 V during undamaged conditions and using two inch diameter, 54kHz transducers, the UGWL arrangement could monitor the physical conditions of an embedded steel bar up to 10 feet long and sensors located up to 25 inches away, illustrated as the red zone in Figure 42.

Table 12. Attenuation coefficient in leakage direction.

Spacing (in)	Difference in amplitude (V)	Attenuation Coefficient		
		(Np/in)	Np/m	dB/m
0.707	-0.0078	-0.1676	-6.598	-57.31
0.707	-0.0046	-0.2225	-8.759	-76.08
0.707	-0.0029	-0.1961	-7.719	-67.05
15.782	-0.0610	-0.2050	-8.069	-70.09
15.782	-0.0251	-0.1682	-6.621	-57.51
15.782	-0.0183	-0.1767	-6.955	-60.41
16.487	-0.0673	-0.2019	-7.950	-69.057
16.487	-0.0297	-0.1705	-6.713	-58.31
16.487	-0.0212	-0.1775	-6.989	-60.71
Average		-0.1898	-7.473	-64.91
Standard deviation		0.0196	0.7083	6.1528

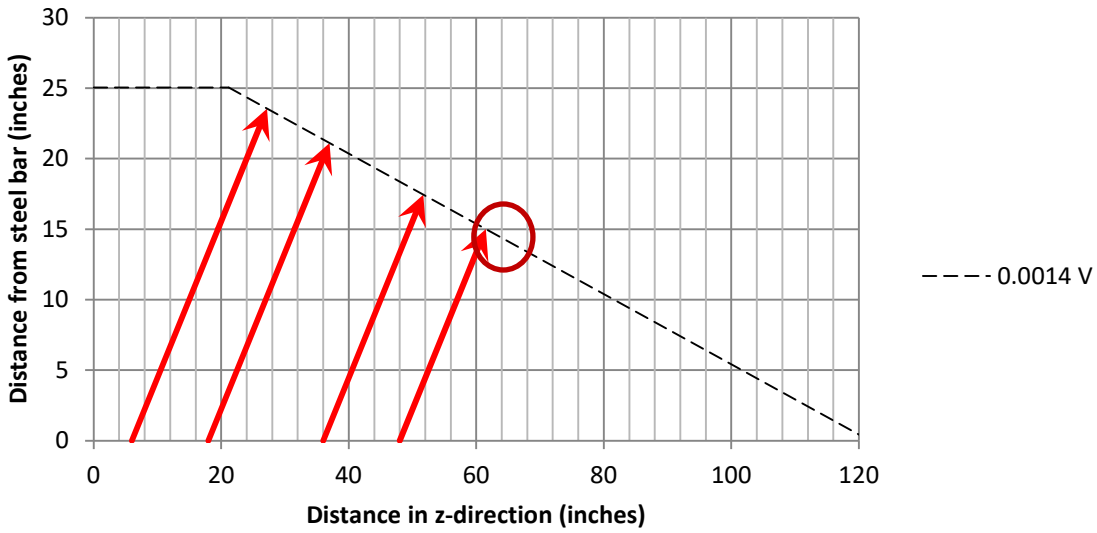

Figure 41. The projected distance sensors should be placed away from steel bar to get the minimum amplitude that this study got from undamaged specimens.

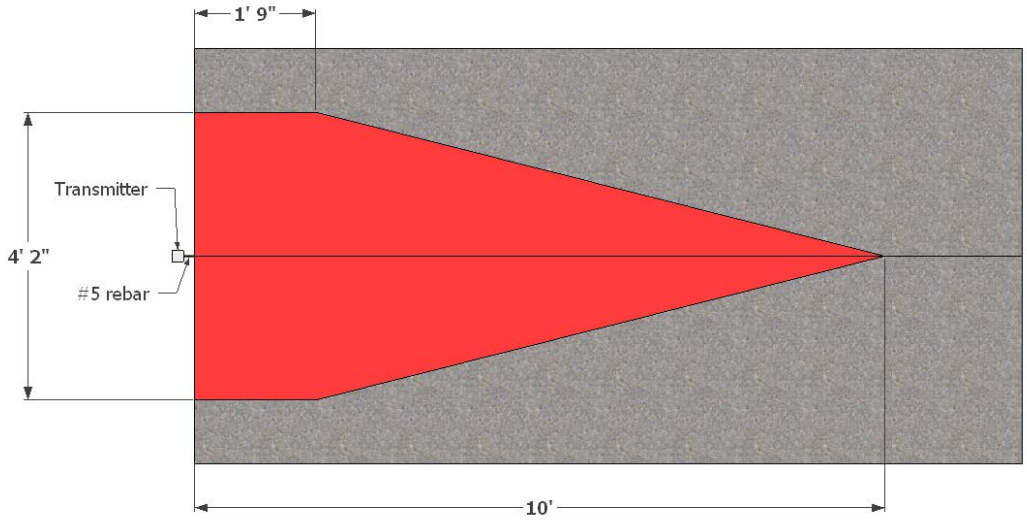

Figure 42. Inspection area of a single transmitter assuming minimal acceptable amplitude of 0.0014V.

Table 13. Sample signal at 61.5 inches in z-direction along sensor array 15 inches from steel bar

	Gain 10 (+20dB)	Gain 1000 (+60dB)
Time Domain	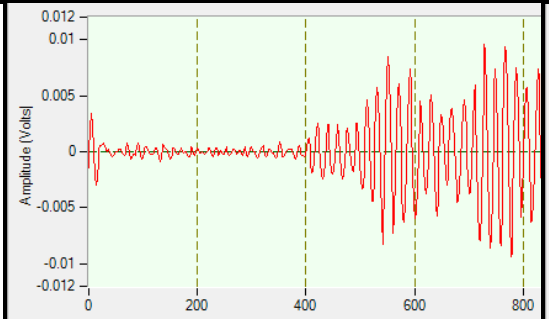	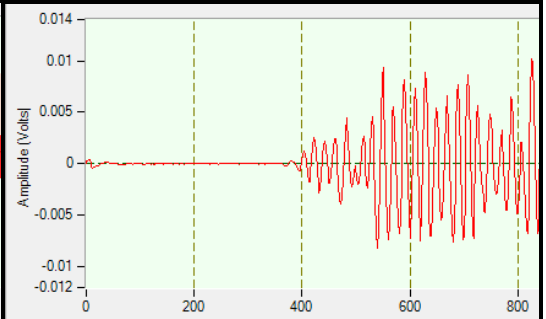
Frequency Domain	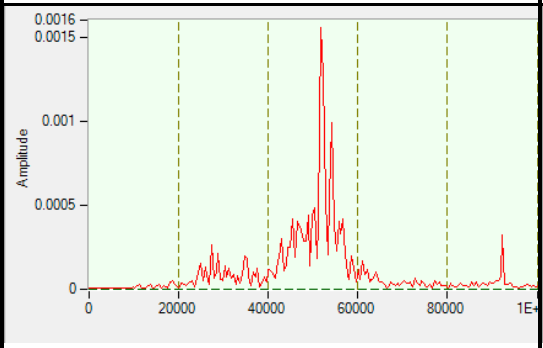	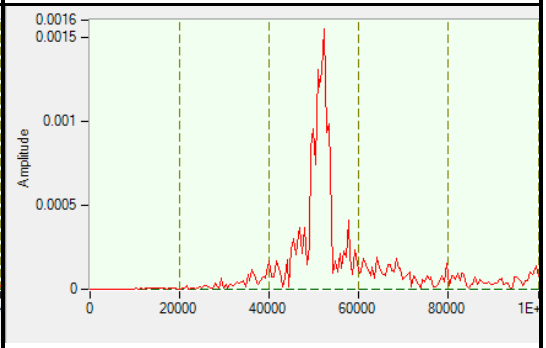

4) Correlation of amplitude and velocity readings of individual sensors with delamination length and width.

In this section, the changes in amplitude and velocity readings at the 6 inch and 12 inch points along the steel bar are presented as these are the only two points monitored that the delamination reached. The transducer locations presented in this discussion come from the arrays at distances of 2.5, 3, and 15 inches. Figure 43 illustrates the conditions observed at the 6 inch and 12 inch points.

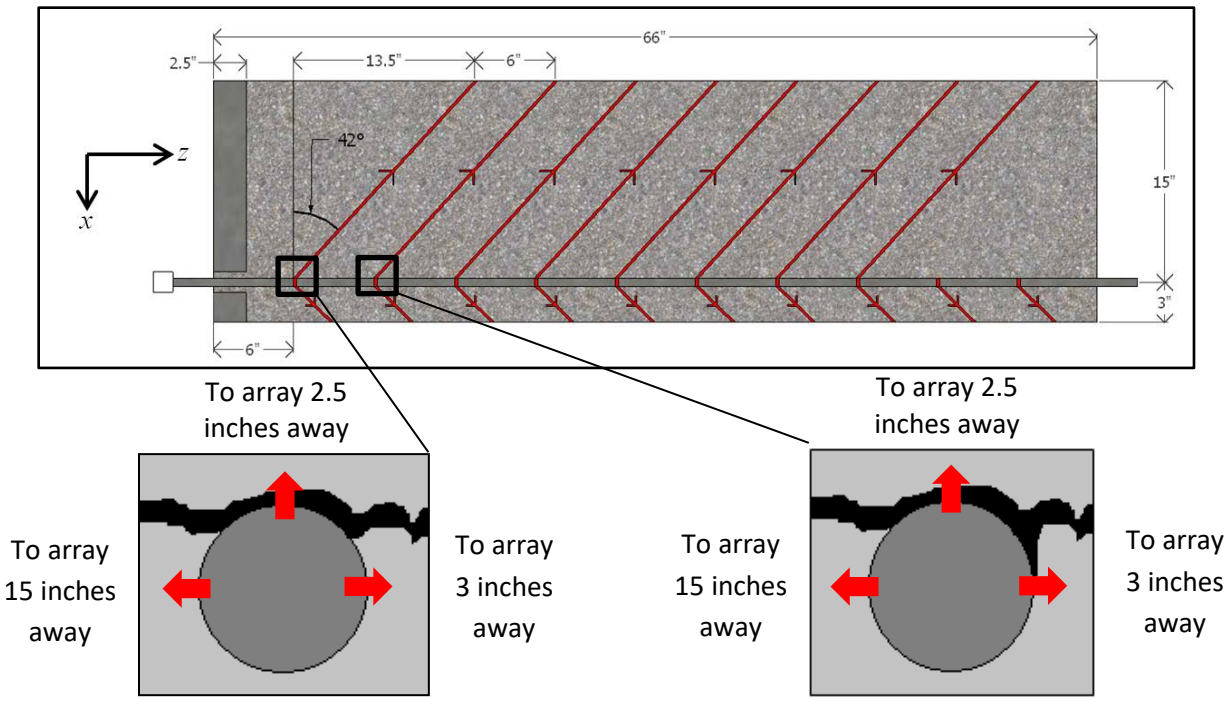

a) 6 inch point along steel bar b) 12 inch point along steel bar

Figure 43. Delamination observed at a) 6 inch point, and b) 12 inch point along steel bar

Delamination lengths were observed and calculated using linear variable differential transformer (LDVT) readings and assuming the crack was linear (Figure 44). Figure 45 shows that the observed lengths matched well with the calculated lengths. Delamination widths were measured using LDVT's located at the start and 3.25 inches in the z-direction. Estimated delamination widths at the 6 inch and 12 inch points in the z-direction were calculated using the LDVT readings and assuming the crack was linear. Figure 46 plots the measured and estimated delamination widths at the 6 inch and 12 inch points, determined using the values shown in Figure 44.

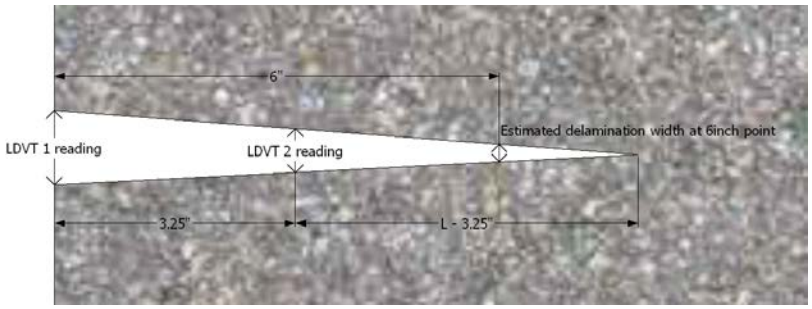

Figure 44.Values used to calculate delamination length, L, and estimated delamination width (assuming linear crack).

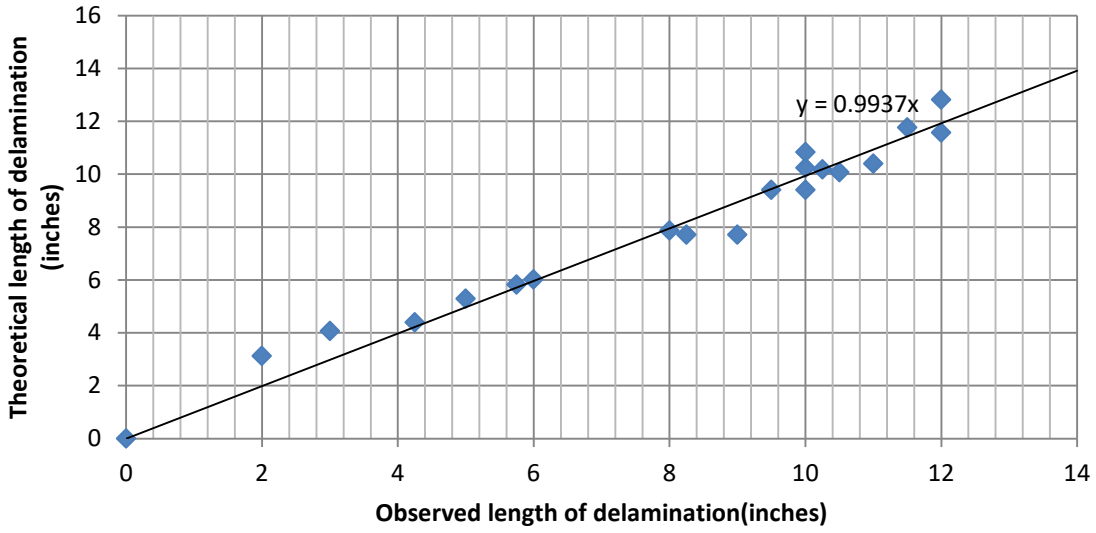

Figure 45. Observed length against theoretical linear crack length.

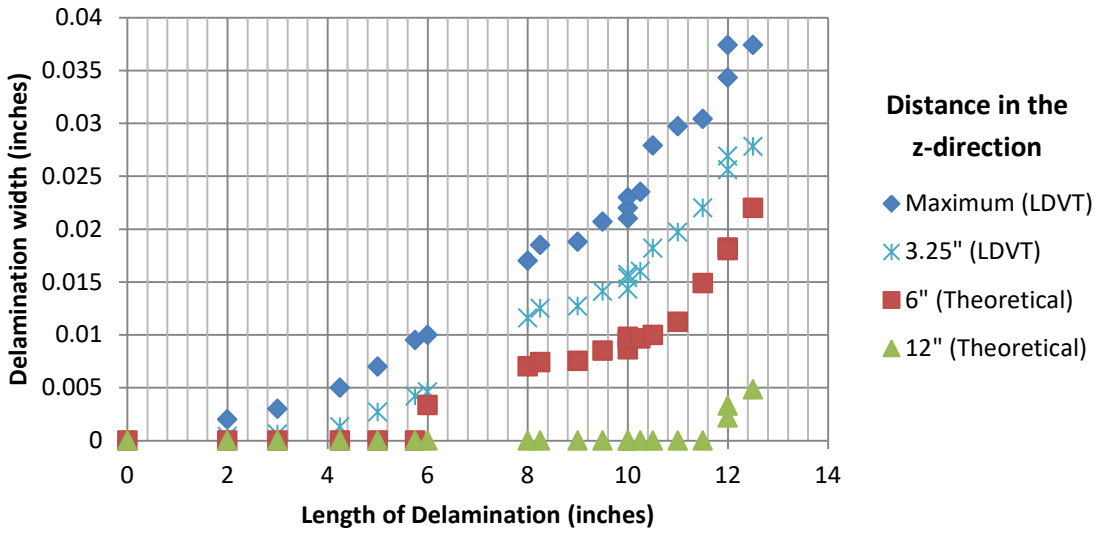

Figure 46. Measured and estimated delamination widths

Figures 47 and 48 illustrate the percent change in velocity at single transducer locations with respect to delamination growth in length and width. These results demonstrate that the length of the delamination can be estimated using velocity readings if the delamination interrupts the path of the leakage to the sensor. If the delamination interrupts the path then the velocity of the signal will decrease, but if a delamination exists and does not interrupt the path then the velocity does not appear to change.

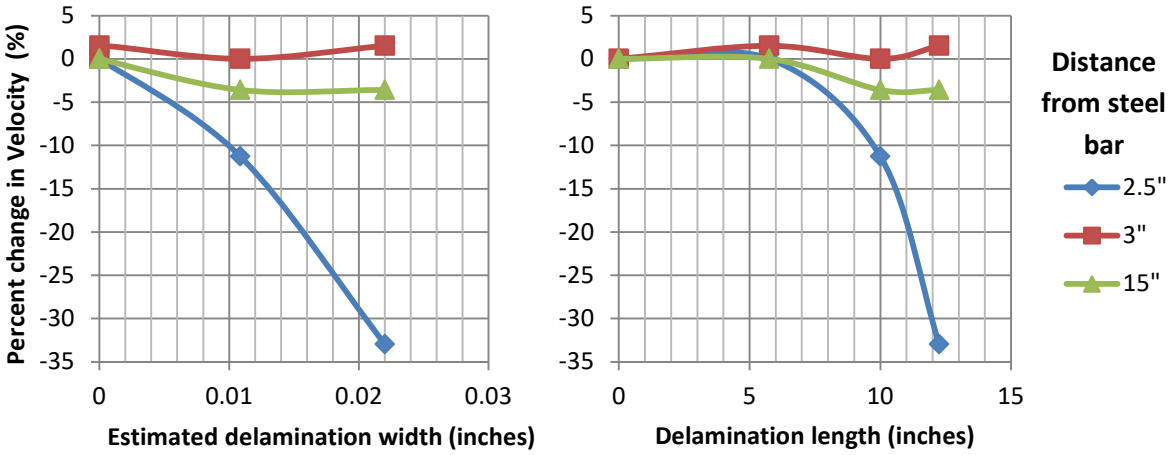

Figure 47. Percent change of velocity with respect to delamination width and length for sensors located to monitor the 6 inch point along steel bar.

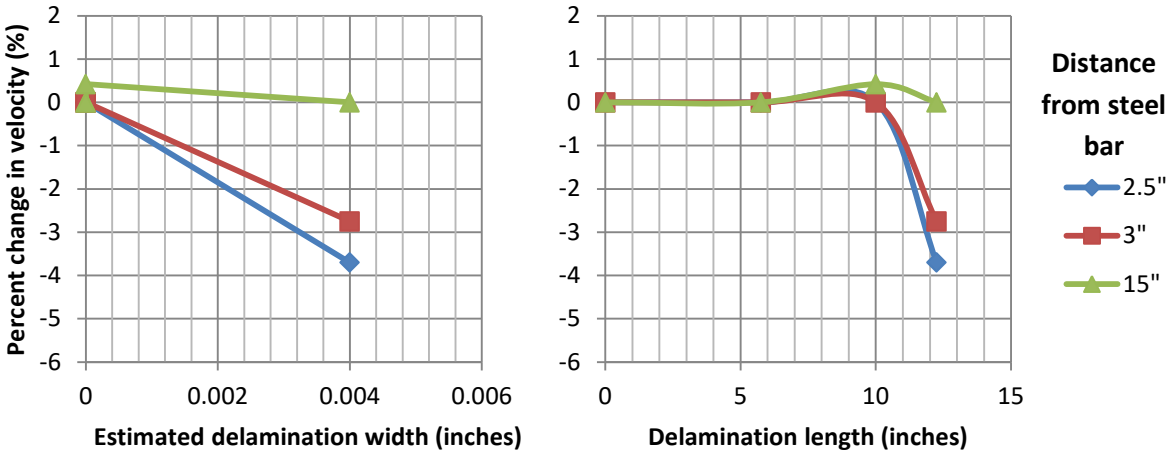

Figure 48. Percent change of velocity with respect to delamination width and length for sensors located to monitor the 12 inch point along steel bar.

Figures 49 and 50 show how amplitude readings at single transducer locations change with respect to delamination growth in length and width. Unlike monitoring the changes in velocity, changes in amplitude readings provide the ability to identify the existence of a delamination regardless of whether it interrupts the path of leakage or not.

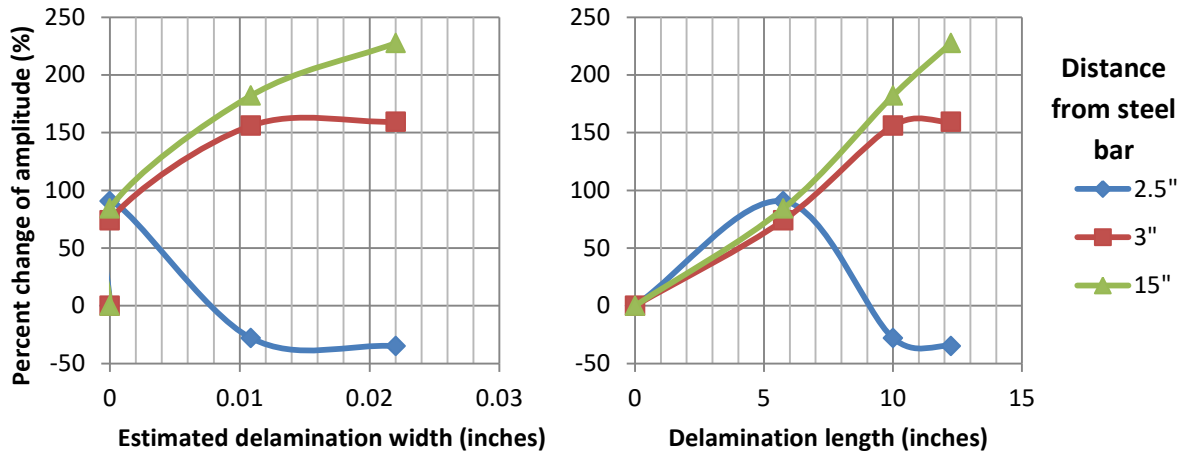

Figure 49. Percent change of amplitude with respect to delamination width and length for sensors located to monitor the 6 inch point along steel bar.

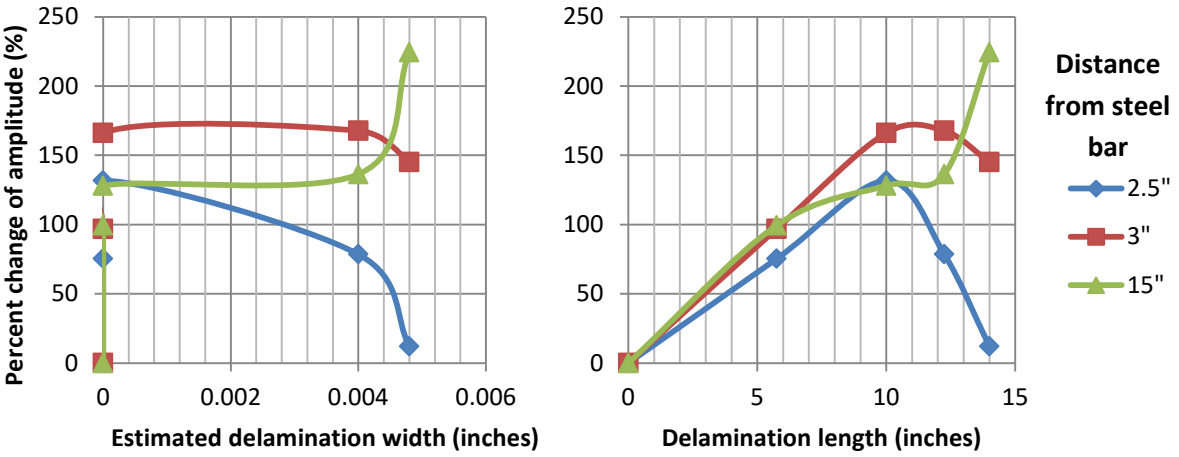

Figure 50. Percent change of amplitude with respect to delamination width and length for sensors located to monitor the 12 inch point along steel bar.

Figure 51 plots the averages with the standard deviations (population of 10 at each delamination width) of the percent changes in amplitude and velocity readings from arrays 2.5, 3 and 15 inches away from the steel bar. The appearance of a correlation suggests that the

percent changes in readings are not influenced by the distance from the steel bar, but only the width of the delamination disrupting the path of leaked waves. Figure 51 clearly illustrates that amplitude measurements are far more sensitive to delamination widths than velocity readings. Figure 51 illustrates that a fitted logarithmic curve of the average percent changes in amplitude fits the correlation between the delamination width and percent change in amplitude. Figure 51 also shows that the correlation between the percent change in velocity measurements and delamination width fits a polynomial curve of second order.

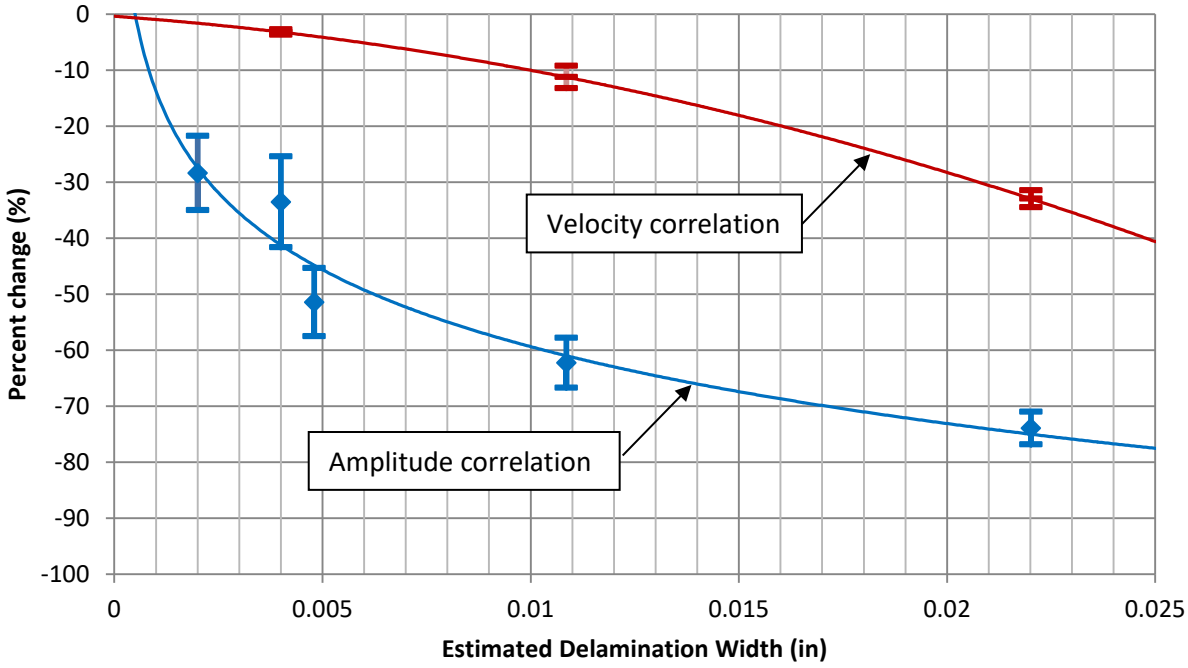

Figure 51. Percent change of amplitude and velocity against estimated delamination width in path of leakage.

5. Conclusions

From the review of literature on current practices and research studies, it was clear that there are significant gaps in structural health monitoring for reinforced concrete bridge decks:

- Currently, there is no NDT-based continuous health monitoring system for delamination in reinforced concrete bridge decks.
- Current NDT methods are unable to identify onset of delamination.
- There are cheaper and more time efficient maintenance techniques that can be used for smaller cracks and delaminations (such as floodcoats), but they are used only if damage can be detected before serious structural issues develop.

It was also found that there is untapped potential with ultrasonic testing, including:

- There are no standardized damage indices for UPA relative to size or degree of damage.
- Currently, there is no UT set-up able to examine or monitor large areas.
- Current UT set-ups are unable to identify type, location, and onset of flaws in the concrete, steel-concrete interface, and steel rebar at once.
- Currently, there is no UT set-up that monitors the leakage of a guided wave.

The **experimental study** demonstrated the feasibility and reliability of using amplitude readings in the frequency domain and a novel UT test set-up measuring UGWL to monitor the onset of delamination.

Specimen set 1 examined the ability to monitor the development and growth of delamination width and provided the following conclusions:

1) All test set-ups demonstrated the ability to identify the onset of delamination/cracks using amplitude readings. All set-ups were able to detect delaminations <0.008". UGW and UGWL are very effective at monitoring the onset of delamination between the steel rebar and concrete interface. UPV direct and indirect set-ups effectively detected micro-delamination in concrete.
2) For all test set-ups, amplitude measurements demonstrated to be at least 10 times more sensitive than velocity measurements to the onset of delamination. Regardless of the rebar condition, path length, or sensor used, the percentage change of amplitude detected correlated with the increase of delamination width. Slight decreases in velocity could occasionally be seen at delaminations 0.0016", but results were not consistent. For the novel UGWL test set-up, amplitude measurements were over 25 times more sensitive than velocity measurements to the onset of delamination.
    a. When delamination 0.008" develops in the path of leakage, amplitude drops by over 50%, compared to velocity only dropping 2%.
    b. When delamination 0.008" develops, but not in the path of leakage, amplitude increases by over 50%, compared to velocity only increasing by less than 1%.
3) Additional leakage caused by the presence of rust propagates through surrounding concrete and can also be detected.

Specimen set 2 further examined the ability of the novel UGWL method and examined its ability to monitor the development and growth of delamination width and length. The summary of the findings from set 2 are as follows:

1) By monitoring the leaked waves from an array of sensor locations, the onset of delamination can be determined and its location along the steel bar can be estimated. This UT approach demonstrated the ability to identify delaminations as small as 2 inches long and 0.002 inches wide that developed close to the transmitter, and were detected by sensors 4 feet away in the z-direction and at a distance of 12.25 inches from the bar. The method also demonstrated the ability to estimate delamination length with data from an array of sensor locations, as well as location of the delamination around the circumference of the embedded steel bar.
2) This experimental study showed that the commonly undesired property of leakage in UT for embedded guided waves can be utilized. The attenuation of the guided wave caused by the surrounding concrete has often been seen as a hindrance to the propagation distance, hence inspection area. However, this study has demonstrated the leaked waves that propagate through the concrete can be monitored and changes in amplitude readings that are influenced by the condition between the steel-concrete interface can be observed. In addition to monitoring 10 feet in the z-direction along the steel bar, the propagation of leaked waves has demonstrated the potential to also monitor the surrounding concrete as clear signals can be detected at distances up to 25 inches on each side of the bar.
3) The development of a delamination had different influences on the change of amplitude and velocity of the leaked waves monitored at each sensor location. Velocity readings monitored at individual sensor locations were only sensitive to delaminations if it disrupted the path of leaked waves to the sensor. When the delamination developed in

the path of leakage to the sensor the velocity readings decreased. Delamination widths around 0.01 inches thick or less caused velocity decreases of around 10% or less, and delaminations around 0.02 inch thick caused velocity readings to drop by 33%. Amplitude readings were sensitive to delaminations regardless of whether the delamination disrupted the path of leaked waves or not. When delamination disrupted the path of leakage the amplitude decreased. Delamination widths of 0.01 inches or less caused amplitude decreases of 65% or less, and delaminations around 0.02 inch thick caused amplitude readings to decrease by 75%. Therefore, it is clear that the changes in amplitude readings are far more sensitive to increases in delamination width than velocity readings, particularly when delamination widths are less than 0.01 inches thick.

Figure 52a combines Figures 24 (specimen set 1) and Figure 51 (specimen set 2), illustrating how the percent changes in velocity and amplitude readings (with respect to delamination width) differed between each set. Specimen set 1 had a consistent delamination length, while specimen set 2 had delamination of varying length as illustrated in Figure 52b. The difference between specimen set 1 and 2 in terms of change in amplitude readings can be explained by the difference in delamination width prior to the region being monitored. These correlations demonstrate the practicality and simplicity of the proposed method. If future work can verify that certain delamination widths correlate with particular changes in amplitude or velocity readings, the onset and size of delamination can be identified at its earliest stages by simply reading how numbers have changed over time.

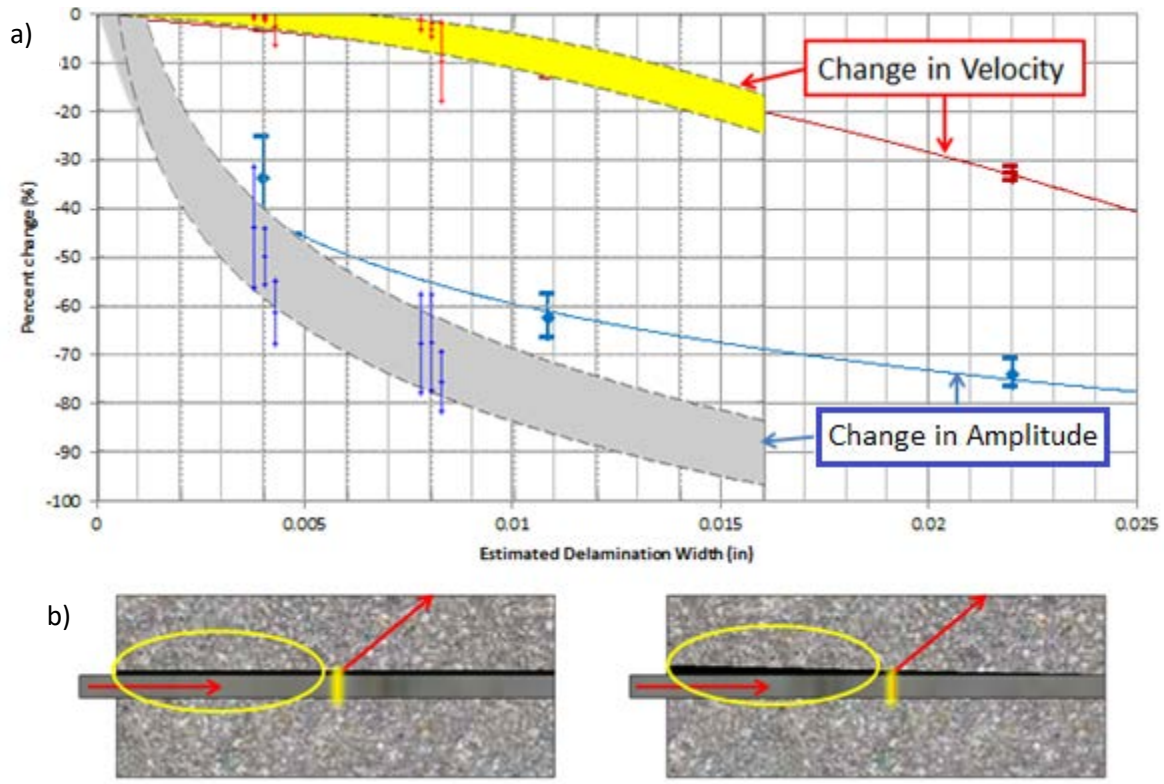

Specimen set 1 Specimen set 2

Figure 52. a) Percent change of amplitude and velocity against estimated delamination width in path of leakage (Specimen sets 1 and 2), b) variation of delamination width.

6. Future Work

A current NDOR project looksto build upon the success of this project (M029) and has two main goals:

1. Expand the application of the method (evaluation of multiple flaws and developing a related diagnostic method).
2. Make it more practical for implementation in real life (propagation distances, optimal sensor arrays, accuracy levels, etc…)

Beyond these two studies, there is also need for further research to ensure practical application of this method. These further research topics include, but are not limited to, appropriate sensor development, field implementation studies, and development of testing standards.

7. References

ACS, 2014. Ultrasonic tomograph for imaging of concrete structures A1040 MIRA [WWW Document]. Acoustic Control Systems. URL http://www.acsys.ru/eng/production/detail/a1040-mira/ (accessed 9.9.15).

Annamdas, V., Yang, Y., Soh, C., 2010. Impedance based concrete monitoring using embedded PZT snesors.pdf. International Journal of Civil and Structural Engineering 1, 11.

ASTM C597-09, 2009. Standard Test Method for Pulse Velocity Through Concrete. ASTM International, West Conshohocken, PA.

Butt, S., Limaye, V., Mufti, A., Bakht, B., 2004. Acoustic Transmission Technique for Evaluating Fatigue Damage in Concrete Bridge Deck Slabs. ACI Structural Journal 101, 9. doi:10.14359/12992

Chen, Y., Wen, Y., Li, P., 2006. Characterization of PZT ceramic transducer embedded in concrete. ScienceDirect - Sensors and Actuators: A 128, 116–124.

Chree, C., 1889. The equations of an isotropic elastic solid in polar and cylindrical coordinates, their solutions and applications, in: Transactions of the Cambridge Philosophical Society. pp. 250–369.

Clemena, G., Lane, S., Freeman, T., Lozev, M., 2000. Evaluation of Nondestructive Evaluation Methods for Application in Early Detection of Deterioration in Concrete Pavements (No. VTRC 00-R13). Virginia Department of Transportation, Charlottesville, Virginia.

Cui, J., Huston, D., Arndt, R., Jalinoos, F., 2012. Multiple Sensor Periodic Nondestructive Evaluation of a Concrete Bridge Deck.

DHS, 2010. Aging Infrastructure: Issues, Research, and Technology, Buildings and Infrastructure Protection Series. Homeland Security - Science and Technology.

Dumoulin, C., Karaiskos, G., Sener, J.-Y., Deraemaeker, A., 2014. Online monitoring of cracking in concrete structures using embedded piezoelectric transducers. IOP 23, 11.

Ervin, B.L., 2007. Monitoring corrosion of rebar embedded in mortar using guided ultrasonic waves (Doctor of Philosophy). University of Illinois at Urbana-Champaign.

FHWA, 2014a. Deficient Bridges by State and Highway System - National Bridge Inventory - Bridge Inspection - Safety - Bridges & Structures - Federal Highway Administration [WWW Document]. Federal Highway Administration - Bridges and Structures. URL https://www.fhwa.dot.gov/bridge/nbi/no10/defbr14.cfm (accessed 9.9.15).

FHWA, 2014b. RABIT Bridge Inspection Tool-- | Federal Highway Administration [WWW Document]. http://www.fhwa.dot.gov. URL http://www.fhwa.dot.gov/research/tfhrc/programs/infrastructure/structures/ltbp/ltbpresearch/rabit/index.cfm (accessed 2.19.15).

Fu, X., Chung, D.D.L., 1997. Effect of corrosion on the bond between concrete and steel rebar. Cement and Concrete Research 27, 1811–1815.

Goueygou, M., Naffa, S.O., Piwakowski, B., Fnine, A., Buyle-Bodin, F., 2002. Measurement of Ultrasonic Attenuation and Rayleigh Wave Dispersion for Testing Concrete with Subsurface Damage. Presented at the IEEE Ultrasonics Symposium, Institute of Electrical and Electronics Engineers.

Hannachi, S., Guetteche, M., 2014. Review of the ultrasonic pulse velocity evaluating compressive strength on site. Presented at the Scientific Cooperations International Workshops on Engineering Branches, Istanbul, Turkey, p. 10.

Hassan, M., Burdett, O., Favre, R., 1993. Combination of ultrasonic measurements and load tests in bridge evaluation, in: Structural Faults + Repair, Infoscience. Presented at the Structural Faults + Repair, EPFL, Edinburgh, UK.

Huang, S., Li, M., Xu, Y., Xu, D., Xie, X., Cheng, X., 2014. Research on Embedded Sensors for Concrete Health Monitoring Based on Ultrasonic Testing, in: ICDCS 2014. Presented at the 4th International Conference on the Durability of Concrete Structures, West Lafayette, IN, p. 5.

Kee, S.-H., Zhu, J., 2013. Using piezoelectric sensors for ultrasonic pulse velocity measurements in concrete. Smart Materials and Structures 22, 115016. doi:10.1088/0964-1726/22/11/115016

Kinsler, L., Frey, A., Coppens, A., and Sanders, J., 2012. Fundamentals of Acoustics, Fourth Edition, John Wiley & Sons Inc.

Krauss, P., Lawler, J., Steiner, K., 2009. GUIDELINES FOR SELECTION OF BRIDGE DECK OVERLAYS, SEALERS AND TREATMENTS (Final Report No. Task234_WJE _Comments 5-19-09), National Cooperative Highway Research Program (NCHRP) Project 20-07. WJE Associates Inc., Illinois.

Kumar, S., Santhanam, M., 2006. Detection of Concrete Damage Using Ultrasonic Pulse Velocity Method, in: Proc. National Seminar on Non-Destructive Evaluation. Presented at the

Proc. National Seminar on Non-Destructive Evaluation, Indian Society for Non-Destructive Testing, India, p. 8.

Landis, E., Shah, S., 1995. Frequency-Dependent Stress Wave Attenuation in Cement-Based Materials. Journal of Engineering Mechanics 121, 737–743.

Lencis, U., Ūdris, A., Korjakins, A., 2011. Decrease of the Ultrasonic Pulse Velocity in Concrete Caused by Reinforcement. Journal of Materials Science and Engineering. A 1, 1016.

Li, D., Ruan, T., JunHui, Y., 2012. Inspection of reinforced concrete interface delamination using ultrasonic guided wave non-destructive test technique. Science China 55, 9.

Li, D., Zhang, S., Yang, W., Zhang, W., 2014. Corrosion Monitoring and Evaluation of Reinforced Concrete Structures Utilizing the Ultrasonic Guided Wave Technique. International Journal of Distributed Sensor Networks 2014, 1–9. doi:10.1155/2014/827130

Lowe, M., Cawley, P., 2006. Long Range Guided Wave Inspection Usage – Current Commercial Capabilities and Research Directions.

Lu, Y., Li, J., Ye, L., Wang, D., 2013. Guided waves for damage detection in rebar-reinforced concrete beams. Construction and Building Materials 47, 370–378.

Miller, T., 2010. Nondestructive Inspection of Corrosion and Delamination at the Concrete-Steel Reinforcement Interface (Doctor of Philosophy). The University of Arizona.

Mustapha, S., Lu, Y., Li, J., Ye, L., 2014. Damage detection in rebar-reinforced concrete beams based on time reversal of guided waves. Structural Health Monitoring 13, 347–358. doi:10.1177/1475921714521268

Naik, T., Malhotra, V., Popovics, J., 2004. The Ultrasonic Pulse Velocity Method, in: HANDBOOK ON NONDESTRUCTIVE TESTING OF CONCRETE. CRC Press LLC, p. 19.

National Research Council (U.S.), Second Strategic Highway Research Program (U.S.), 2013. Nondestructive testing to identify concrete bridge deck deterioration, SHRP 2 report. Transportation Research Board, Washington, D.C.

Na, W.-B., Kundu, T., Ehsani, M., 2003. Lamb Waves for Detecting Delamination between Steel Bars and Concrete. Computer-Aided Civil and Infrastructure Engineering 18, 58–63.

Niederleithinger, E., Wolf, J., Mielentz, F., Wiggenhauser, H., Pirskawetz, S., 2015. Embedded Ultrasonic Transducers for Active and Passive Concrete Monitoring. Sensors 15, 9756–9772. doi:10.3390/s150509756

Pavlakovic, B., 1998. Leaky Guided Ultrasonic Waves in NDT. University of London, London.

PCA, 2002. Types and Causes of Concrete Deterioration (No. IS536). Portland Cement Association.

Pochhammer, L., 1876. Uber die fortpflanzungsgeschwindigkeiten kleiner schwingungen in einem unbegrenzten isotropen kreiszylinder. Journal f¨ur die Reine und Angewandte Mathematik 81, 324–336.

Popovics, J., Rose, J., 1994. A survey of developments in ultraonic NDE of concrete. IEEE Transactions on Ultrasonics, Ferroelectrics, and Frequency Control 41, 140=143.

Poston, R., 2008. Structural Concrete Repair, in: Concrete Construction Engineering Handbook. CRC Press, pp. 16.1–16.41.

RILEM TC, 1994. NDT 1 Testing of concrete by the ultrasonic pulse method, 1972, in: RILEM Recommendations for the Testing and Use of Constructions Materials. E & FN SPON, pp. 73 – 82.

Rogers, C., Bouvy, A., Schiefer, P., 2011. Thin Epoxy Overlay and Healer Sealer Treatments on Bridge Decks.

Rose, J., 2003. Dispersion curves in guided wave testing. Materials Evaluation 20–22.

Rose, J., 2002. A Baseline and Vision of Ultrasonic Guided Wave Inspection Potential. ASME 124, 273–282.

Rose, J.L., 1999. Ultrasonic waves in solid media. Cambridge University Press, Cambridge ; New York.

Sabnis, G., Kelishami, R., Millstein, L., 1990. Delamination detection in concrete bridge decks usting ndt test method, in: Proceedings of Nondestructive Evaluation of Civil Structures and Materials. Presented at the Nondestructive Evaluation of Civil Structures and Materials, Boulder, CO, pp. 371–380.

Santhanam, M., 2010. Ultrasonic Characterization of Damage in Concrete. Structural Longevity 3, 111–125.

Shah, A.A., Hirose, S., 2009. Nonlinear ultrasonic investigation of concrete damaged under uniaxial compression step loading. Journal of Materials in Civil Engineering.

Silk, M., Bainton, K., 1979. The propagation in metal tubing of ultrasonic wave modes equivalent to Lamb waves. Ultrasonics 17, 11–19.

Song, G., Gu, H., Mo, Y.L., Hsu, T.T.C., Dhonde, H., 2007. Concrete structural health monitoring using embedded piezoceramic transducers. Smart Materials and Structures 16, 959–968. doi:10.1088/0964-1726/16/4/003

Streeter, K., 2002. Ultrasonic Attenuation Tomography of Concrete Structures (Masters Thesis). University of Colorado, Colorado.

Suaris, Fernando, 1987. Ultrasonic Pulse Attenuation as a Measure of Damage Growth during Cyclic Loading of Concrete [WWW Document]. URL http://www.scribd.com/doc/240524528/Ultrasonic-Pulse-Attenuation-as-a-Measure-of-Suaris-1987#scribd (accessed 9.19.15).

Sun, H., & Zhu, J. (2017). Monitoring Early Age Properties of Cementitious Material Using Ultrasonic Guided Waves in Embedded Rebar," Journal of Nondestructive Evaluation, in press. DOI: 10.1007/s10921-016-0383-3

Treiber, M., Kim, J.-Y., Qu, J., Jacobs, L., 2010. Effects of sand aggregate on ultrasonic attenuation in cement-based materials. RILEM 43, 1–11.

Virmani, Y.P., Clemena, G., 1998. FHWA-RD-98-088--CORROSION PROTECTION - CONCRETE BRIDGES (Final Report No. FHWA-RD-98-088). Federal Highway Administration.

Vogt, T., 2002. Determination of Material Properties Using Guided Waves (Doctor of Philosophy). University of London - Imperial College of Science, Technology and Medicine, London.

Wang, Y., Zhu, X., Hao, H., Ou, J., 2009. Guided wave propagation and spectral element method for debonding damage assessment in RC structures. Journal of Sound and Vibration 324, 751–772. doi:10.1016/j.jsv.2009.02.028

Wu, F., Chang, F.-K., 2006. Debond Detection using Embedded Piezoelectric Elements for Reinforced Concrete Structures - Part II: Analysis and Algorithm. Structural Health Monitoring 5, 17–28. doi:10.1177/1475921706057979

Yunovich, M., Thompson, N., Balvanyos, T., Lave, L., 2001. Corrosion Cost and Preventive Strategies in the United States, Appendix D—Highway Bridges (No. FHWA-RD-01-157). Federal Highway Administration.

Zheng, Z., Lei, Y., 2014. Effects of Concrete on Propagation Characteristics of Guided Wave in Steel Bar Embedded in Concrete. Shock and Vibration 2014, 1–14. doi:10.1155/2014/910750

Zheng, Z., Lei, Y., Xue, X., 2014. Numerical Simulation of Monitoring Corrosion in Reinforced Concrete Based on Ultrasonic Guided Waves. The Scientific World Journal 2014, 1–9. doi:10.1155/2014/752494

Zhu, J., 2008. Non-contact ndt of concrete structures using air coupled sensors. Newmark Structural Engineering Laboratory. University of Illinois at Urbana-Champaign.

Zhu, X., Hao, H., 2009. Debond detection in RC structures using piezoelectric materials, in: Concrete Repair, Rehabilitation and Retrofitting II. CRC Press, Boca Raton [Fla.]; London.

8. APPENDIX A

The following figures show samples of data presented in Table 8.

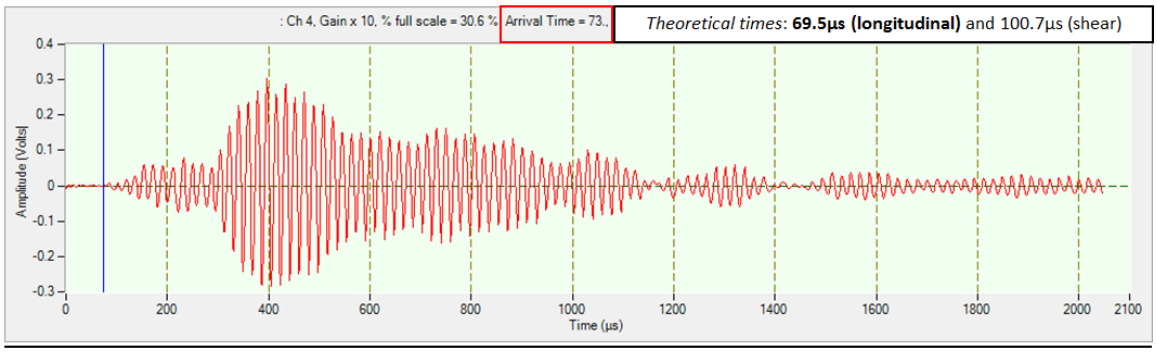

Figure A.1 – Sensor located 6 inches on concrete in z-direction (see Table 8)

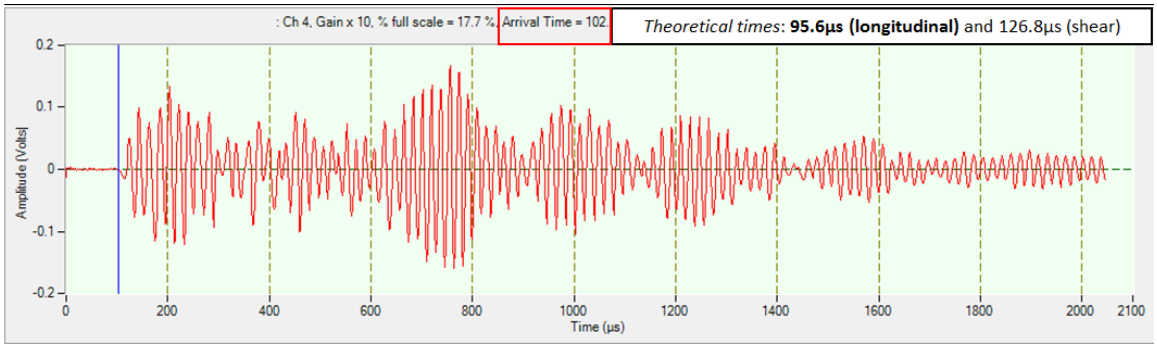

Figure A.2 – Sensor located 12 inches on concrete in z-direction (see Table 8)

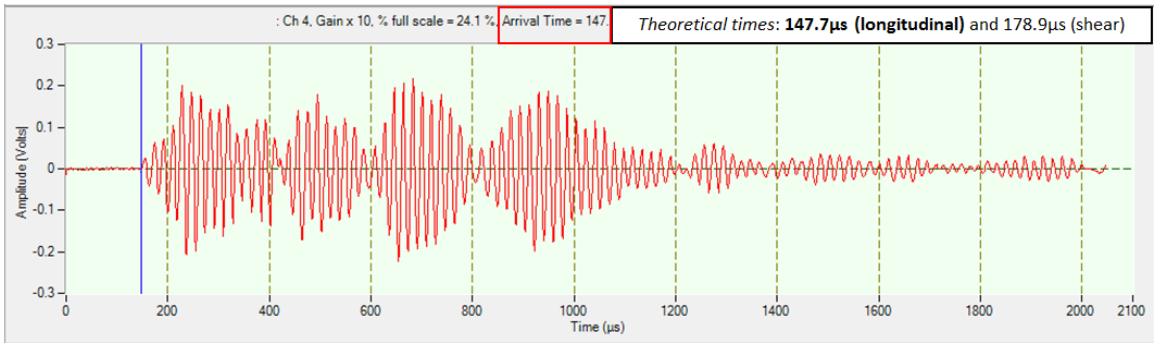

Figure A.3 – Sensor located 24 inches on concrete in z-direction (see Table 8)

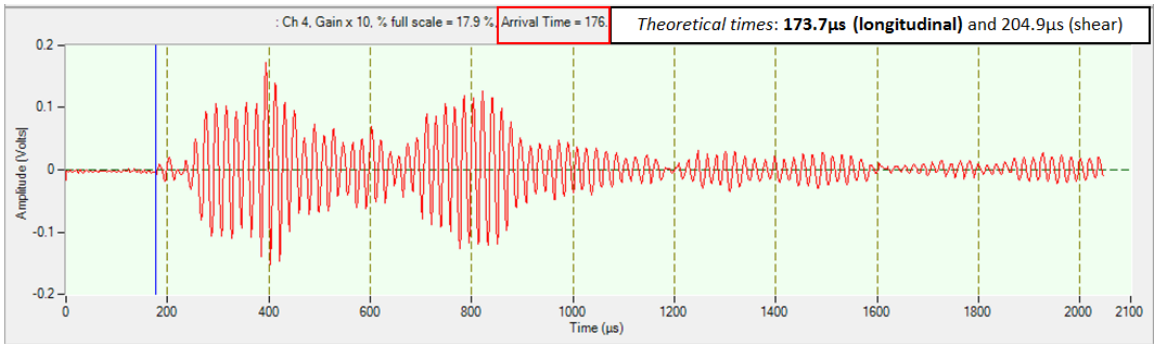

Figure A.4 – Sensor located 30 inches on concrete in z-direction (see Table 8)

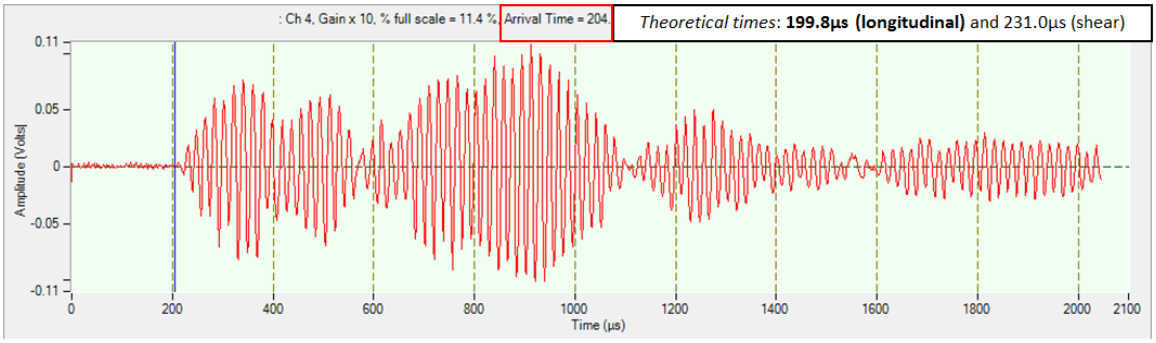

Figure A.5 – Sensor located 36 inches on concrete in z-direction (see Table 8)

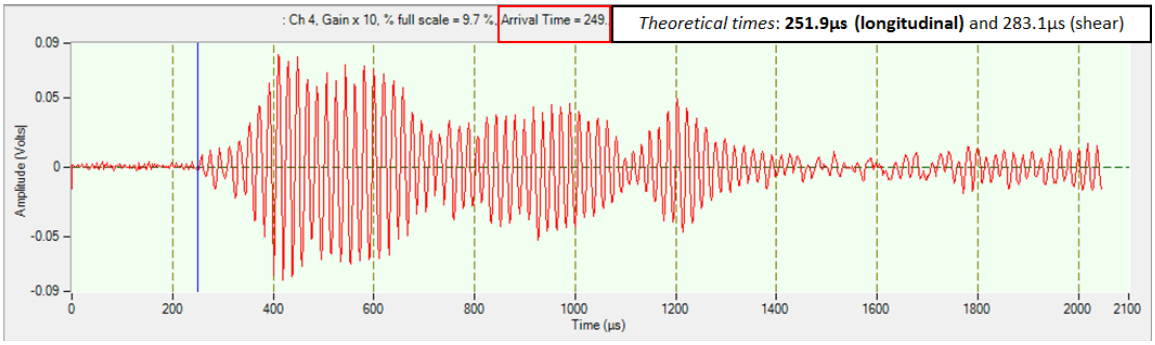

Figure A.6 – Sensor located 48 inches on concrete in z-direction (see Table 8)

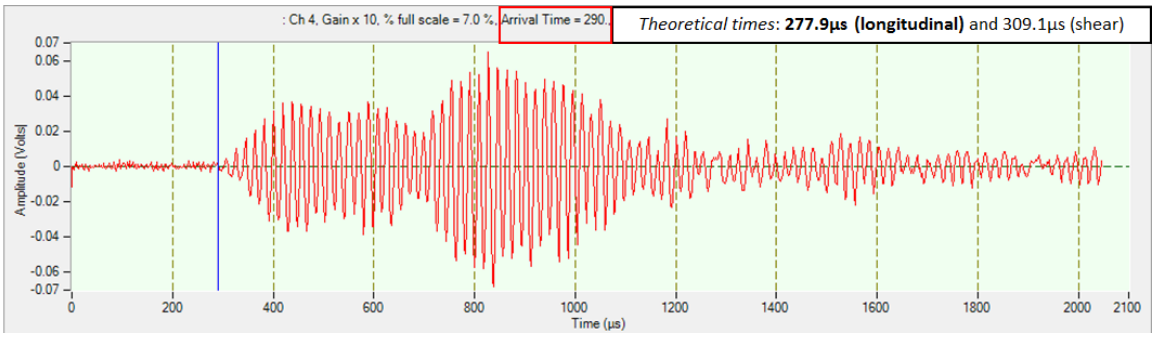

Figure A.7 – Sensor located 54 inches on concrete in z-direction (see Table 8)

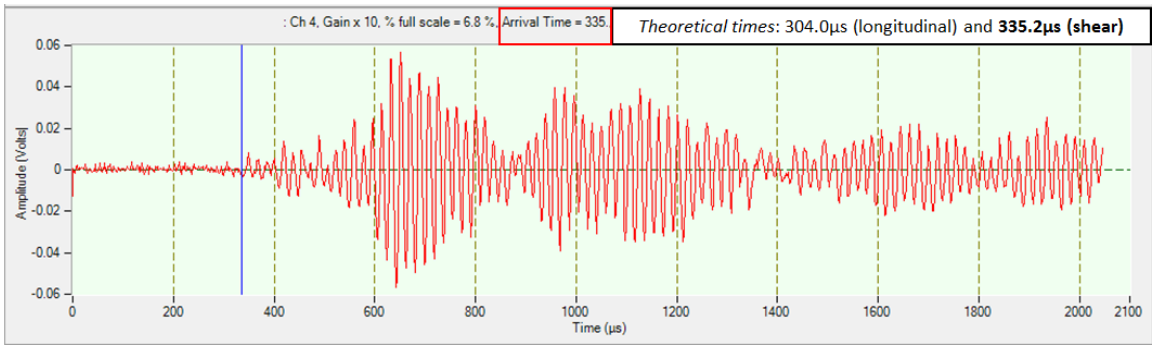

Figure A.8 – Sensor located 60 inches on concrete in z-direction (see Table 8)

APPENDIX B

The following figures show samples of data presented in Table 9.

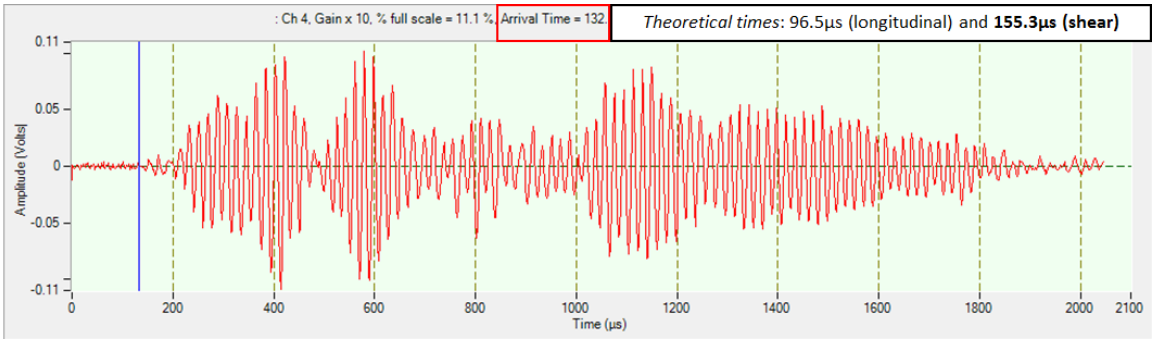

Figure B.1 – Sensor located 6 inches on concrete in z-direction (see Table 9)

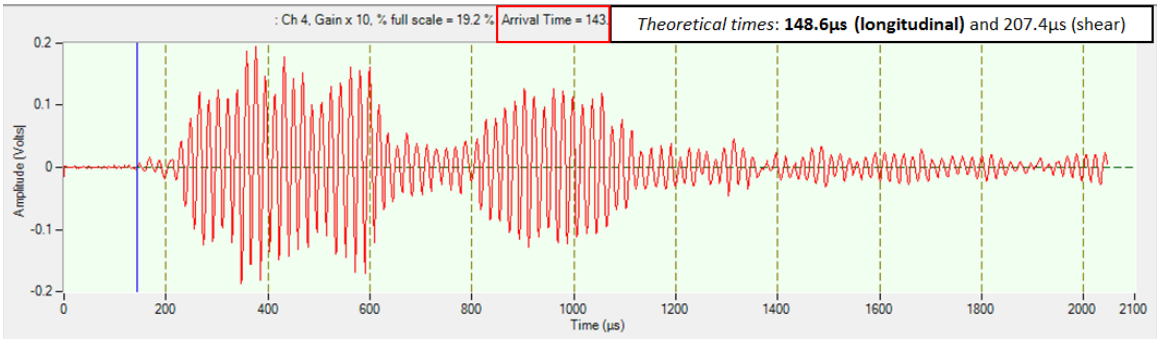

Figure B.2 – Sensor located 18 inches on concrete in z-direction (see Table 9)

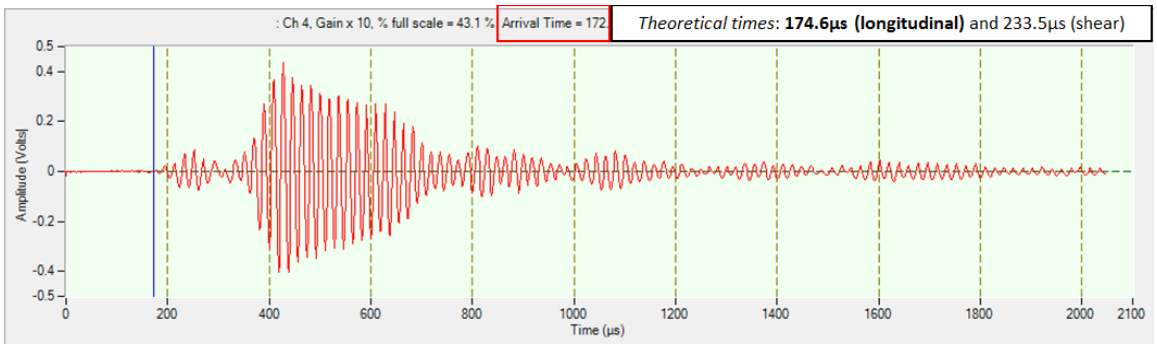

Figure B.3 – Sensor located 24 inches on concrete in z-direction (see Table 9)

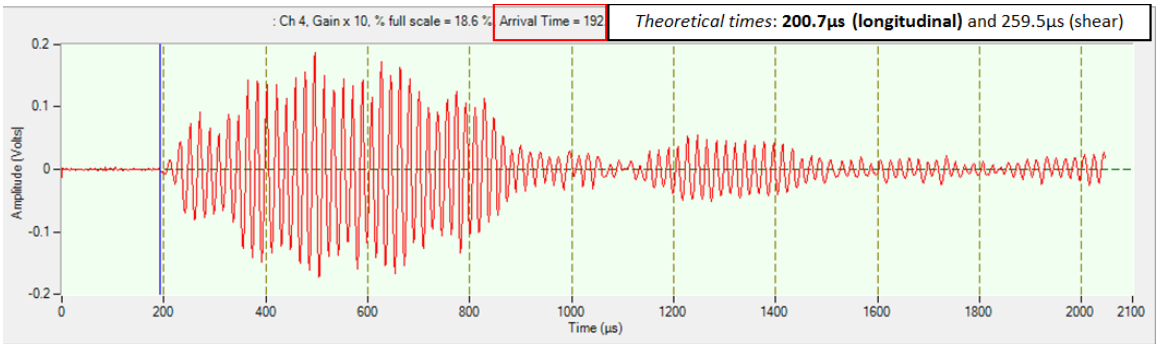

Figure B.4 – Sensor located 30 inches on concrete in z-direction (see Table 9)

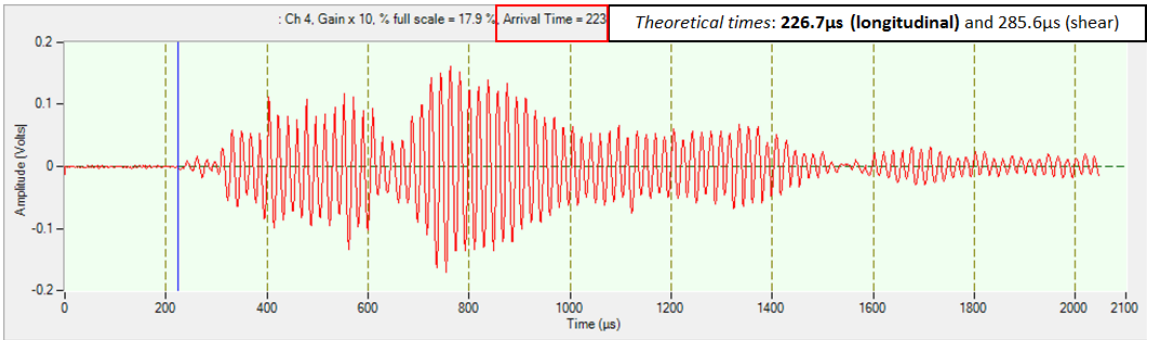

Figure B.5 – Sensor located 36 inches on concrete in z-direction (see Table 9)

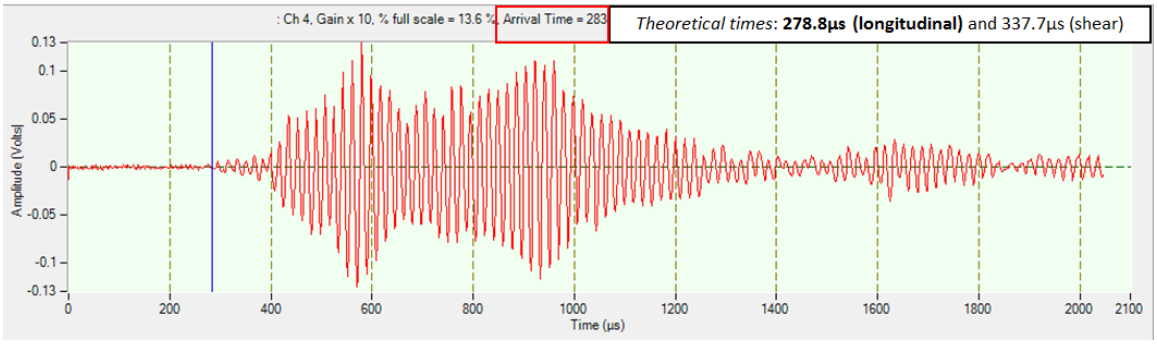

Figure B.6 – Sensor located 48 inches on concrete in z-direction (see Table 9)

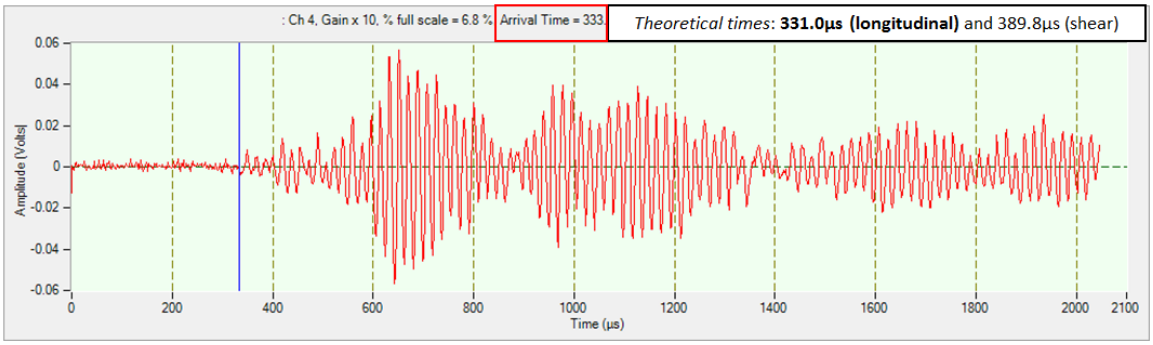

Figure B.7 – Sensor located 60 inches on concrete in z-direction (see Table 9)